

SOFTWARE VALIDATION TEST PLAN AND REPORT FOR ANSYS-FLUENT VERSION 12.1

Prepared for

**U.S. Nuclear Regulatory Commission
Contract NRC-02-07-006**

Prepared by

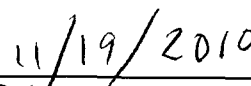
**Kaushik Das
Debashis Basu
Center for Nuclear Waste Regulatory Analyses
San Antonio, Texas**

November 2010

Approved by:



David A. Pickett



Date

CONTENTS

Section	Page
FIGURES	iv
TABLES	vi
1 INTRODUCTION	1-1
1.1 Scope of Validation.....	1-3
1.2 Natural and Forced Convection.....	1-4
1.3 High Speed Flows	1-5
1.4 Radiation Heat Transfer	1-5
1.5 Multiphase Flows.....	1-6
2 ENVIRONMENT	2-1
2.1 Software	2-1
2.2 Hardware	2-2
3 PREREQUISITES	3-1
4 ASSUMPTIONS AND CONSTRAINTS.....	4-1
5 NATURAL AND FORCED CONVECTION.....	5-1
5.1 Natural Convection in an Annulus Between Horizontal Concentric Cylinders	5-1
5.1.1 Theoretical Basis	5-2
5.1.2 Test Input.....	5-3
5.1.3 Expected Test Results.....	5-3
5.1.4 Test Results.....	5-3
5.2 Natural Convection Along a Vertical Flat Plate.....	5-6
5.2.1 Theoretical Basis	5-6
5.2.2 Test Input.....	5-7
5.2.3 Expected Test Results.....	5-8
5.2.4 Test Results.....	5-8
5.3 Flow Over Back-Facing Step.....	5-10
5.3.1 Theoretical Basis	5-11
5.3.2 Test Input.....	5-13
5.3.3 Expected Test Results.....	5-13
5.3.4 Test Results.....	5-13
5.4 Flow and Heat Transfer Over Expansion Pipe	5-16
5.4.1 Theoretical Basis	5-17
5.4.2 Test Input.....	5-17
5.4.3 Expected Test Results.....	5-18
5.4.4 Test Results.....	5-18

CONTENTS

Section	Page
6	HIGH SPEED FLOWS 6-1
6.1	Flow Over Wedge 6-1
6.1.1	Theoretical Basis 6-2
6.1.2	Test Input 6-3
6.1.3	Expected Test Results 6-4
6.1.4	Test Results 6-4
6.2	Turbulent Mixing Layer of Compressible Flow 6-6
6.2.1	Theoretical Basis 6-6
6.2.2	Test Input 6-7
6.2.3	Expected Test Results 6-7
6.2.4	Test Results 6-7
7	RADIATION HEAT TRANSFER 7-1
7.1	Radiation Between Two Parallel Surfaces 7-1
7.1.1	Theoretical Basis 7-2
7.1.2	Test Input 7-2
7.1.3	Expected Test Results 7-3
7.1.4	Test Results 7-3
7.2	Radiation Between Two Concentric Cylinders 7-4
7.2.1	Theoretical Basis 7-5
7.2.2	Test Input 7-6
7.2.3	Expected Test Results 7-6
7.2.4	Test Results 7-7
8	SPECIES TRANSPORT AND MULTIPHASE FLOWS 8-1
8.1	Diffusion Through Mixture Column at Constant Pressure and Temperature 8-1
8.1.1	Theoretical Basis 8-2
8.1.2	Test Input 8-3
8.1.3	Expected Test Results 8-4
8.1.4	Test Results 8-4
8.2	Condensation of Water Vapor Over Flat Plate 8-6
8.2.1	Theoretical Basis 8-7
8.2.2	Test Input 8-9
8.2.3	Expected Test Results 8-9
8.2.4	Test Results 8-10
8.2.4.1	Test Results for Single-Phase Species Transport ... 8-10
8.2.4.2	Test Results for Multiphase Transport with Volumetric Condensation 8-12
9	INDUSTRY EXPERIENCE 9-1
10	NOTES 10-1
11	REFERENCES 11-1

FIGURES

Figure	Page
5-1	Computational Domain for Kuehn and Goldstein Problem..... 5-1
5-2	Velocity Vectors and Temperature Contours for Different Rayleigh Numbers..... 5-5
5-3	Computational Domain and Grid for Natural Convection Over Vertical Heated Plate. 5-6
5-4	Velocity Vectors and Temperature Contours (a) of the Domain and (b) Near the Exit 5-9
5-5	Comparison of Computed and Analytical Values of Nusselt Number Where the Upper and Lower Limit of Acceptance is Within 10 Percent of Computed Value. (a) Version 12.1 and (b) Version 6.3 5-10
5-6	Velocity and Temperature Distribution at the Plane A-A. (a) Version 12.1 and (b) Version 6.3 5-10
5-7	Computational Domain, Grid, and Boundary Conditions for Back-Facing Step..... 5-11
5-8	Velocity Near the Vicinity of the Back-Facing Step. (a) Version 12.1 and (b) Version 6.3..... 5-14
5-9	Turbulent Kinetic Energy Near the Vicinity of the Back-Facing Step. (a) Version 12.1 and (b) Version 6.3..... 5-14
5-10	Comparison of Computed Skin Friction Coefficient With Experimental Data. (a) Version 12.1 and (b) Version 6.3..... 5-15
5-11	Comparison of Computed Pressure Coefficient With Experimental Data (a) Version 12.1 and (b) Version 6.3..... 5-15
5-12	Computational Domain Grid and Boundary Conditions for Flow and Heat Transfer Over Expanded Pipe 5-16
5-13	Velocity, Temperature, and Turbulent Kinetic Energy in the Flow Field Using Version 12.1 5-19
5-14	Comparison of Experimental and Computed Nu/Nu_{DB} Along the Heated Wall..... 5-19
6-1	Features of Supersonic Flows Over Wedge..... 6-1
6-2	Domain, Grid, and Boundary Conditions for Flow Over Wedge..... 6-2
6-3	Simulated Density Field Using FLUENT Version 12.1 6-4
6-4	Simulated Pressure Field Using FLUENT Version 12.1 6-5
6-5	Comparison of Analytical and Computed Solutions Along the Floor (a) Mach Number and (b) Density Ratio 6-5
6-6	Computational Domain, Grid, and Boundary Conditions for Compressible Mixing Layer 6-6
6-7	Velocity Distribution in the Mixing Layer..... 6-8
6-8	Turbulent Kinetic Energy Distribution in the Mixing Layer..... 6-8
6-9	Comparison of Computed and Experimental Turbulent Kinetic Energy at $x = 100$ mm 6-9
6-10	Comparison of Computed and Experimental Axial Velocity at $x = 100$ mm 6-9

FIGURES

Figure	Page
7-1	Schematic of Radiation Heat Transfer Between Parallel Surfaces 7-1
7-2	Temperature Contours Across the Gap Using DO Model in FLUENT Version 12.1 7-3
7-3	Comparison of Analytical and Computed Solution of Temperature Across the Gap Along with the Acceptance Limit of ± 10 Percent Using DO Model for FLUENT Version 12.1 7-4
7-4	Schematic of Radiation Heat Transfer Between Concentric Cylinders 7-5
7-5	Temperature Contours Annulus Using S2S Model in FLUENT Version 12.1 7-7
7-6	Comparison of Analytical and Computed Solution of Temperature Across The Annulus Using FLUENT Version 12.1 7-8
8-1	Schematic of Diffusion in Mixture Column..... 8-1
8-2	Water Vapor Mass Fraction Variation in the Flow Field Using (a) Version 12.1 and (b) Version 6.3 8-4
8-3	Comparison of Analytical and Computed Solution of Mass Fraction Of Water Vapor. (a) Version 12.1 and (b) Version 6.3 8-5
8-4	Comparison of Analytical and Computed Solution of Mass Fraction Of Air. (a) Version 12.1 and (b) Version 6.3 8-6
8-5	Schematic for Condensation of Humid Air Over Flat Plate 8-7
8-6	Air Mass Fraction Variation in the Flow Field 8-11
8-7	Comparison of Analytical and Computed Results for Condensation Mass Flux for Inlet Velocity. (a) Equals 0.1 m/s and (b) Equals 1 m/s 8-11
8-8	Relative Humidity Contours for Simulation with Single-Phase Species Transport and Inlet Velocity = 1 m/s..... 8-11
8-9	Air Mass Fraction Variation in the Flow Field with Multiphase Flow and Inlet Velocity = 1 m/s 8-12
8-10	Comparison of Analytical and Computed Results for Condensation Mass Flux for Inlet Velocity Using Multiphase Flow Modeling. (a) Equals 0.1 m/s and (b) Equals 1 m/s 8-12
8-11	Relative Humidity Contours for Simulation with Multiphase Species Transport and Inlet Velocity = 1 m/s..... 8-13

TABLES

Table	Page
5-1	Selected Experiments for FLUENT Simulations..... 5-3
5-2	Properties of Nitrogen for FLUENT Simulation Conditions 5-3
5-3	Mesh Sizes for Grid Independence Study for FLUENT..... 5-3
5-4	Comparison of Measured and Predicted Equivalent Thermal Conductivity for Concentric Cylinders 5-4
5-5	Comparison of Measured and Predicted Equivalent Thermal for Three Grid Levels 5-5
5-6	Flow Parameters for Flow Over a Back-Facing Step 5-11

1 INTRODUCTION

ANSYS-FLUENT® Version 12.1¹ is a general purpose computational fluid dynamics software package developed by ANSYS Inc. It is widely used for design and analysis of applications ranging from aircraft components to sporting goods and garments. It is among the leading computer-aided engineering tools that engineers predominantly use for flow, chemistry, and heat transfer simulations in a continuum, though it has some added modules for magnetohydrodynamics and discrete particle problems. Industry reports, trade journals, and technical literature show that it is regularly used in the automobile industry, bio-fluids applications, electronic cooling in the semiconductor industry, high speed flows over aircraft wings and fuselage, multiphase flows in the nuclear industry, and turbomachinery flow simulations in rotating frames of reference.

The FLUENT software was initially developed by Fluent Inc., which was subsequently acquired by ANSYS Inc. ANSYS has combined a number of engineering analysis software, such as ANSYS-Mechanical, ANSYS-Meshing, and the computer-aided design (CAD) package Design Modeler (DM), to create an integrated workbench. In this integrated workbench, each software tool coexists as a separate entity, but users can select tools they need to address a particular problem on a seamlessly integrated platform, where data and information from one package is communicated automatically to others. For example, if an engineer is interested in combined thermal and mechanical analysis of a pipe flow system that carries high temperature fluid, he can use DM to do the solid modeling, ANSYS Meshing to discretize the domain and then ANSYS-Mechanical and FLUENT to perform the structural and fluid analysis in a coupled fashion with minimal user interaction. The process of creating an integrated benchmark is still underway. Before ANSYS Inc. acquired FLUENT, Geosciences and Engineering Division (GED) staff used FLUENT Version 6.3, which had undergone the validation and verification process (Das and Basu, 2007). After the merger, FLUENT Inc. stopped supporting Version 6.3 and GED staff switched to the ANSYS-FLUENT Version 12.1. The new version retained almost all the features of the older Version 6.3 and has some added capabilities. GED staff have also adopted the new integrated platform mentioned previously (ANSYS-Workbench) to perform simulation activities. However, GED currently retains a license only for the computational fluid dynamics (CFD) packages within the Workbench platform and presently does not perform any combined analysis that requires packages such as ANSYS-Mechanical.

FLUENT solves the generalized Navier-Stokes equations using the finite volume technique. It has a pressure- and a density-based solver to solve the incompressible and compressible flows, respectively. The standard version of FLUENT has a comprehensive suite of models to represent conduction, convection, and radiation heat transfer with options to simulate phase change and solidification-melting phenomena. A number of multiphase flow modeling techniques, including the volume of flow method, Eulerian-Eulerian model, mixture model, and the discrete particle tracking methods, are available in the solver. The standard solver can be customized to meet the requirements unique to a particular application by using the “user-defined functions.” There are a number of added modeling tools that are available within the FLUENT

¹ANSYS-FLUENT® Version 12.1 will be referred to as FLUENT in this document.

framework, along with the generalized flow solver, meant for analyzing specialized problems. For example, an automobile engineer can use the discrete particle model and the chemistry toolbox of FLUENT to study in-cylinder combustion of an engine, the heat exchanger module to design a radiator, and the pollutant module to assess the level of emissions from the exhaust gas. Similarly, FLUENT can be used to study external aerodynamics of an aircraft body and the specialized models to investigate gas turbine combustion and turbomachinery flows.

FLUENT uses an unstructured grid and supports a number of grid elements, such as hexahedral, polyhedral, prismatic, and tetrahedral mesh. The solver employs the Message Passing Interface (MPI) routines for parallel processing in a number of platforms including Microsoft® Windows® NT, UNIX, and different variants of LINUX. FLUENT has the dynamic and moving mesh capabilities required for specialized flows, such as in-cylinder flows in internal combustion engines, valves, store separation, and release of objects from aircrafts. Users can choose from a number of turbulence models ranging from zero equation models to large eddy simulation techniques available with the standard solver to simulate turbulence as their problems require. A number of spatial discretization schemes, like the first-order upwind scheme, power law scheme, second-order upwind scheme, and central differencing scheme, are available with both implicit and explicit time integration techniques for temporal terms of the equations. The simulation boundary conditions could be defined using the options available with the solver, or users can define them through customized functions. Most of the standard boundary conditions, such as the velocity and pressure inlet boundaries, outflows, periodic conditions, and solid wall conditions, are available with the standard package. A large database of fluid and solid properties is also provided with the solver to model the presence of fluids, solids, and mixtures. Special boundary conditions and numerical treatment needed for swirling and rotating flows and flows with nonstationary reference frames can be input as user options in the solver.

Previously, a separate grid generator and preprocessor called GAMBIT Version 2.4² was used for preprocessing activities. These activities include development of the geometry and grid generation. The GAMBIT preprocessor was also used to define boundary conditions and different fluid and solid materials and export the mesh for use in FLUENT simulations. Currently, the ANSYS Workbench has the CAD package DM and ANSYS-Meshing for building geometry and creating grids. Additionally, a postprocessor called CFD-POST is available for visualization of simulated results.

The validation study documented in this report for FLUENT covers the technical areas where the software has been applied to GED activities. Validation is done through the method of regression, where the case and data files from the previous versions are used to verify whether the new version is producing results within the acceptable limit. This validation report supersedes the previous versions.

The code was employed to perform a number of tasks involving thermal analysis of engineered and natural systems in potential high-level waste repository drifts at

²GAMBIT® Version 2.4 will be referred to as GAMBIT in this document.

Yucca Mountain and to support other experimental and analytical work that the Center for Nuclear Waste Regulatory Analyses (CNWRA®) performs. These tasks include

- Perform supporting calculation and independent verification of existing simulations of in-drift thermal environment, air flow, and moisture transport caused by the dissipation of decay heat from the radioactive waste and availability of liquid water in the drift wall
- Numerically simulate magma–waste package interaction in the event of a volcanic eruption in potential high-level waste repository drifts at Yucca Mountain
- Simulate the high speed viscous flow and heat transfer processes during magma ascent and propagation through dikes
- Develop and perform detailed erosion corrosion simulation of nuclear power plant components
- Perform high speed water flow simulations through dams and spillways and subsequently use the cavitation model of FLUENT to study spillway damage
- Perform flow analysis in the near-borehole area through fractured porous rocks for feedback to structural analysis
- Support calculation related to aerosol migration through the atmosphere in the near-coastal region
- Validate and verify the VSC-17 thermal model against experimental data
- Apply the thermal model to a proof-of-concept canister for storage, transportation, and transfer canisters
- Perform thermal hydraulic simulation of nuclear power reactor components

In addition, FLUENT could be used as a tool to support and supplement other experimental and analytical work that involves fluid flow and heat transfer.

1.1 Scope of Validation

As mentioned previously, the method of regression will be used to perform the validation exercise. validation simulations will focus on the following areas only.

- Natural and forced convection
- High speed flows
- Radiation heat transfer
- Multiphase flows and species transport

These four categories cover the broad technical area where CNWRA intends to use the code. If needed, other physical models available in FLUENT will be validated based on the problem requirements. Users are advised to perform relevant tests pertinent to their specific needs when applying FLUENT to technical areas that are not validated here.

The validation test cases are summarized in the following subsections. The input and output files for each validation test case are included in the attached electronic media.

1.2 Natural and Forced Convection

The natural and forced convection simulation capabilities of FLUENT are validated through four test cases that are described in Chapter 6. The first two test cases relate to free or natural convection, and the subsequent two test cases are associated with forced convection and heat transfer. The four test cases are summarized next.

- Natural convection between two concentric cylinders: Kuehn and Goldstein (1978, 1976) performed a series of experiments to investigate the thermal behavior of a gas in an annulus between concentric circular cylinders. The experimental results from this study will be used to validate FLUENT for both laminar and turbulent natural convection simulations as required by the potential use of the software.
- Natural convection along a vertical flat plate: Analytical solution of transport equations for natural convection flow over a vertical, flat, heated plate is well documented (Incropera and Dewitt, 1996). A test case is set up to replicate the problem, and the computed results are compared with the analytical solution.
- Flow over back-facing step: This test case is used to validate FLUENT for forced convection flows. The test case is modeled after the Driver and Seegmiller (1985) experimental investigation that studied incompressible turbulent flow over a rearward-facing step in a diverging channel flow. The measured and computed skin friction and pressure coefficients are matched as a part of the validation exercise.
- Flow and heat transfer over an expansion pipe: The experiment Baughn, et al. (1984) conducted to measure the local heat transfer coefficient downstream of an abrupt expansion in a circular channel is used as a benchmark to validate the capability of FLUENT in simulating forced convection flows. Computed Nusselt number distribution along the channel wall is compared with experimental data.

The forced convection test cases described in this section are relevant to the erosion corrosion studies that are being performed at GED. The natural convection studies are relevant to storage and disposal of spent nuclear fuel. The ventilation airflow around storage canisters usually creates a transitional or turbulent natural convection flow, whereas the backfill gas inside the canister may have natural convection. These test cases are also relevant to in-drift flow, moisture, and heat transfer processes. During the preclosure period, forced convection conditions are experienced due to active ventilation. In the postclosure period, in the absence of any active ventilation, the flow field is perturbed by the heated waste package and a natural convection flow starts in presence of gravitational force.

1.3 High Speed Flows

The test cases described in Chapter 7 validate the FLUENT code for application in high speed flows. Two test cases are considered in the validation exercise of high speed flows.

- Flow over wedge: The analytical solution for supersonic flow over a wedge can be obtained from the theory of inviscid flows and oblique shocks as Anderson (1984) documented. The high speed supersonic flow contacts the leading edge of the ramp and generates an oblique shock, where the flow properties exhibit a sharp discontinuity. A hypothetical test case is built to simulate the supersonic flow over a 15° wedge, and the results are compared with the analytical solution.
- A detailed experimental study of the compressible turbulent mixing layer by Goebel and Dutton (1991) is used to validate the solver capability in computing compressible flows. Two fluid streams with different velocities are injected inside a rectangular chamber, where the turbulent mixing process takes place. The experimental investigation measured the turbulent kinetic energy and axial velocity profiles that are compared with simulated results.

The test cases described in this section will be relevant in modeling fragmented magma flow in the dike and drift in a potential volcanic eruption at the potential high-level waste repository drifts at Yucca Mountain. Fragmented magma flow inside the drift is generally considered as a compressible fluid and characterized by the presence of shocks, viscous interactions, and turbulence. Magmatic ascent of fluid through the dike could also be modeled as internal compressible flow. In addition, the water flow through the spillways and overflowing dams will use some of the FLUENT simulation techniques.

1.4 Radiation Heat Transfer

Two simple test cases are considered to validate the radiation models of FLUENT in Chapter 8. FLUENT has a number of models to simulate radiation including complex scenarios like scattering, particle–radiation interaction, optical media thickness, gray gas, and specular reflection. The test cases for the present validation exercise are restricted to modeling physical features that are relevant to the intended application [e.g., surface-to-surface (S2S) radiation with nonparticipating media.] The test cases considered for radiation heat transfer follow.

- Radiation between two parallel surfaces: One-dimensional analytical solution of radiation heat transfer between two parallel plates is well known (Incropera and Dewitt, 1996; Holman, 2002). This hypothetical test case test assumes no convective air flow in between the surfaces. The computed results are compared with analytical solution of temperature distribution and heat flux.
- Radiation between two concentric cylinders: Analytical solution of radiation heat transfer between two concentric cylinders is well documented in open literature (Incropera and Dewitt, 1996; Ozisik, 1977). The fluid inside the annulus is maintained at very low pressure to simulate a vacuum. The computed temperature distribution and heat flux across the annulus will be compared with an analytical solution.

Radiation will be the dominant mode of heat transfer in dry storage casks due to the high temperature of the spent fuel caused by decay heat. The test cases described here validate the models that will be required to simulate radiation in enclosed surfaces with inert, nonparticipating media as typically encountered in the casks. These test cases are also relevant to the simulation of the in-drift environment during the postclosure period because the radiation heat transfer will contribute significantly to the overall heat transfer rate.

1.5 Multiphase Flows

Two test cases to simulate multispecies flows of air–vapor mixtures are considered and described in Chapter 9. The first test case is suitable for modeling evaporation columns where a fixed mass fraction of a species is maintained across boundaries. The second test case deals with forced convection flow of moist air over a cold flat plate resulting in phase change. The test cases are

- Diffusion through a mixture column at constant temperature and pressure: A binary gas mixture of water vapor and air fills a rectangular box at a constant temperature and pressure, where water vapor diffuses across the domain in the presence of a concentration gradient. The analytical solution of this hypothetical problem under a steady-state condition is provided in the open literature (Bird, et al., 1960; Incropera and Dewitt, 1996), which is used as a basis for validating FLUENT. The analytical solution for species concentration across the rectangular domain is matched with predicted results.
- Condensation of water vapor over a flat plate: Sparrow, et al. (1967) have analytically determined the condensed mass of liquid water formed over a flat plate due to flow of humid air. The validation test case models flow of an air–water vapor mixture at different velocities over a flat plate and simulates the condensation process through suitable source terms in the transport equations. This test case will also be simulated using a modified user subroutine that models volumetric condensation to achieve equilibrium in the flow domain. Simulated condensate mass distribution along the floor is compared with analytical solution.

Validation test cases for multiphase flows are highly relevant for simulation of the erosion–corrosion process inside pipelines. In addition, it will be applicable in modeling magma–waste package interaction that involves phase change. Multiphase flows could also be used to model the magma behavior inside the dike and drift during the posteruption period. Validated phase change and species transport simulation techniques are also relevant to the postclosure performance in a repository drift that is characterized by moisture transport, evaporation, and condensation. The in-drift moisture redistribution analysis performed by the U.S. Department of Energy uses the species transport model of FLUENT (Bechtel SAIC Company, LLC, 2004).

2 ENVIRONMENT

2.1 Software

The FLUENT software package was developed in the early 1980s and is the flagship software of Fluent Inc.—a company that spun off from the New Hampshire-based research and development firm Creare, Inc. As mentioned in Chapter 1, Fluent Inc. was acquired by ANSYS Inc., which developed an integrated platform to perform a range of engineering analyses.

Since its inception as a general purpose fluid dynamics software, a host of models has been added to the original flow solver that could address a wide range of industrial applications. The flow solver can model combustion, reacting flows, turbomachinery flows, multiphase flows, aeroacoustics, heat transfer, and a number of other flow problems. The physical models available in FLUENT are detailed in the FLUENT User's Guide (ANSYS Inc., 2009a). The Fluent Inc. website (www.fluent.com) also illustrates various examples and test cases of flow modeling applications for industrial problems.

The present validation exercise will be carried out in the LINUX operating system—specifically on Red Hat Enterprise Linux, Version 5.0. ANSYS Workbench preprocessors, Design Modeler and ANSYS-Meshing, will be used to generate the geometry and meshes used in the validation study. The preprocessor is evoked from LINUX by activating the graphical user interface (GUI) and proper selection of simulation options. The preprocessor and its methods of use are detailed in the ANSYS-Design modeler users guide (ANSYS Inc., 2009c) and ANSYS Meshing Users Guide (ANSYS Inc., 2009d). The main flow solver FLUENT can also be evoked either from the GUI or from a console by typing “fluent” at the command prompt. The in-build postprocessor for the Workbench is called CFD-Post and can also be evoked from either the Workbench GUI or from the console by typing “cfdpost.” Details on how to use CFD-Post are available from the CFD-Post Users Guide (ANSYS Inc., 2009e). FLUENT creates two files—namely, the case and data files—that store the grid information and flow parameters, respectively. The flow parameters that are being stored in the data file depend on the physical models that are being invoked in the solution and are determined by the software without any specific user input. Computational fluid dynamic simulations often take many hours or even days to complete; hence, users should retain files holding simulation results for future analyses and postprocessing.

The standard version of FLUENT has the option to include customized routines tailored to model-specific applications. The routines are known as user-defined functions that are compiled and dynamically linked to the standard solver. They are written in the C programming language using any standard text editor, and the source code file is saved with a *.c extension*. One source file can contain a single user-defined function or multiple user-defined functions, or a number of source files could be used to build one user-defined function depending on the complexity of the problem. Licensing constraints are detailed in the license agreement.

2.2 Hardware

FLUENT supports a number of platforms and operating systems that include Windows XP and Windows 2000 as well as different varieties of UNIX, including SOLARIS 9.0 and 10.0, HP-UX 11.23, AIX 5.2, and IRIX 6.5. FLUENT also supports a variety of LINUX operating systems including SuSE and RedHat. It can be used on both 32- and 64-bit architecture. The software is capable of performing parallel processing and uses different techniques to communicate between processors, including the standard MPI. It can use shared memory as well as distributed memory machines for parallel activities. The parallel processing capabilities are available in Windows NT, LINUX, and UNIX platforms.

The present validation study will be conducted in the CNWRA LINUX cluster (Katana). The cluster has 64-bit processors and presently has 18 computer nodes.

3 PREREQUISITES

Users should be trained to use FLUENT and have experience in fluid mechanics and heat transfer.

4 ASSUMPTIONS AND CONSTRAINTS

FLUENT is currently installed in the cluster Katana and the stand alone machine Niagra. Because of license requirements, it can only be used on these machines. Usage is restricted by the terms and conditions in the license agreement, which restricts redistribution of the software. The validation studies proposed here could also be used for installation testing of the software.

5 NATURAL AND FORCED CONVECTION

The test cases described in this section validate the FLUENT Version 12.1 code for application in natural and forced convection. The first two test cases relate to free or natural convection and are similar to the validation test cases for the flow solver FLOW-3D[®] documented in Green and Manepally (2006). The final two test cases validate the flow solver for forced convection and heat transfer.

5.1 Natural Convection in an Annulus Between Horizontal Concentric Cylinders

A well-reported experiment by Kuehn and Goldstein (1978) is used as a benchmark for validating FLUENT 6.3 for simulating natural convection flows. The experimental study measured temperature and heat flux of a gas in an annulus between concentric and eccentric circular cylinders. For the present validation study, only the concentric configuration is considered. The scientific community has used this experimental study to validate computational fluid dynamics calculations of natural convection flows. The validation simulations use nitrogen as the gas in the annulus to match the experimental conditions. Other physical parameters were chosen to replicate the test conditions that are described in Section 5.1.2.

The experiment facility consisted of two concentric cylinders sealed in a pressure vessel. The outer diameter of the inner cylinder was 3.56 cm, and the inner diameter of the outer cylinder was 9.25 cm, resulting in an annular gap of 2.845 cm. The cylinders were

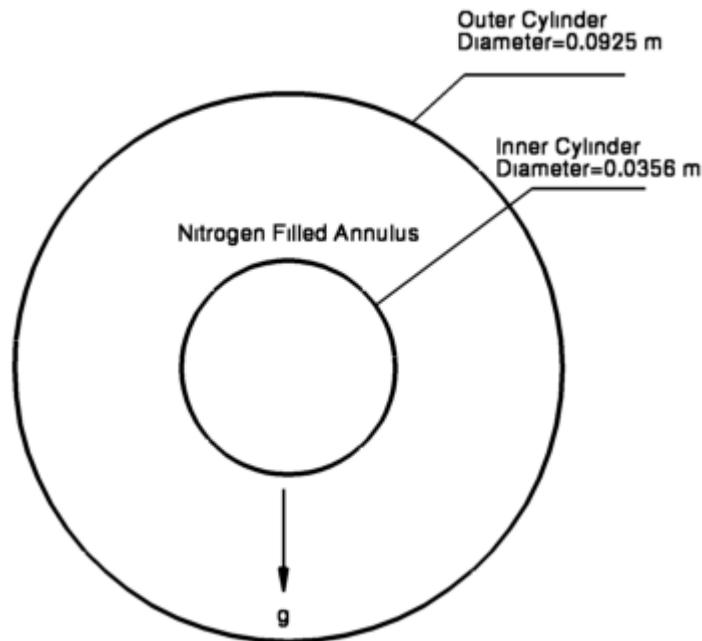


Figure 5-1. Computational Domain for Kuehn and Goldstein Problem

20.8 cm in length. The inner cylinder was electrically heated, while the outer cylinder was cooled with a chilled water loop to maintain constant temperature conditions at the walls. The test chamber was filled with nitrogen as the test fluid. The nitrogen pressure was varied between 0.071 atm and 35.2 atm, and the temperature difference between the two cylinders was varied between 0.83 K and 60.1 K. This provided for a Rayleigh number range of 2.2×10^2 to 7.74×10^7 . Temperatures in the annulus were measured via Mach-Zender interferometry, and surface temperatures were measured with thermocouples.

5.1.1 Theoretical Basis

A hypothetical physical property—equivalent thermal conductivity—was used to reduce the experimental data. It is the conductivity value that would result in equal heat flux across the annulus if conduction were the only mode of heat transfer. The equivalent thermal conductivity between the inner and outer cylinder was calculated for different test conditions. The equivalent thermal conductivity is defined as

$$K_{eff} = \frac{Q \ln\left(\frac{D_o}{D_i}\right)}{2\pi k \Delta T} \quad (5-1)$$

where

Q	—	Heat transfer rate at inner cylinder per unit length (W/m)
D_o	—	Diameter of the outer cylinder (m)
D_i	—	Diameter of the inner cylinder (m)
k	—	Thermal conductivity of the gas in the annulus (W/m-K)
ΔT	—	Temperature difference between the inner and outer cylinder (K)

The experimental study calculated the effective thermal conductivity for different test conditions that resulted in different flow patterns. These different test conditions could be expressed in terms of the nondimensional parameter Rayleigh number, which is given by

$$Ra = \frac{g\beta\Delta TL^3 Pr}{\nu^2} \quad (5-2)$$

where

β	—	Thermal expansion coefficient of gas (1/K)
ν	—	Kinematic viscosity of the gas in the annulus (m ² /s)
Pr	—	Prandtl number of the gas
g	—	Acceleration due to gravity (m/s ²)
L	—	Characteristic length = $0.5(D_o - D_i)$ (m)

Simulation results for the present validation study are conducted under similar conditions and the effective thermal conductivity values are calculated from the simulated results that are compared against the experimental values.

5.1.2 Test Input

FLUENT mesh files are generated to mimic the experimental setup by Kuehn and Goldstein (1978) in a two-dimensional (2D) domain. Two sets of studies are conducted for this validation test case. In the first set of tests, the FLUENT solver is used to simulate three different flow conditions that correspond to three different Rayleigh numbers. The physical parameters used to simulate these three Rayleigh numbers are described in Table 5-1, and the corresponding properties of nitrogen are described in Table 5-2. The input parameters are the same as those in Das and Basu (2008).

A second set of studies was conducted to perform a grid independence test of the results. Three levels of mesh resolution are considered. The grid independence study is conducted for the Rayleigh number of 1.31×10^3 , and the physical parameters corresponding to that Rayleigh number are used for all three tests. Table 5-3 provides the details of the mesh used in this study. Input for all the test cases is on the attached media in the directory named K-g-12.1/.

Table 5-1. Selected Experiments for FLUENT Simulations

Rayleigh Number	P (atm)	ΔT (°C)	$\frac{1}{2}(T_i + T_o)$ (°C)	Flow Regime
1.31×10^3	0.110	53.5	51.1	Laminar
2.51×10^6	34.6	0.91	27.7	Transitional
6.60×10^7	35.0	28.7	40.8	Turbulent

Table 5-2. Properties of Nitrogen for FLUENT Simulation Conditions

Rayleigh Number Ra	ρ kg/m ³	β 1/K	μ Pa-sec	Cp J/(kg-K)	k W/(m-K)	FLUENT Input File Name
1.31×10^3	0.1158	3.08×10^3	1.903×10^5	1,033.37	0.0274	K-G-lam.cas
2.51×10^6	39.40	3.323×10^3	1.859×10^5	1,041.07	0.02793	K-G-tran.cas
6.60×10^7	38.07	3.185×10^3	1.916×10^5	1,040.67	0.02874	K-G-turb.cas

Table 5-3. Mesh Sizes for Grid Independence Study for FLUENT

Rayleigh Number	Total Number of Nodes	Level of Resolution	FLUENT Input File Name
1.31×10^3	120,800	Fine	k-g-fine.cas
1.31×10^3	3,700	Medium	k-g-medium.cas
1.31×10^3	500	Coarse	k-g-coarse.cas

5.1.3 Expected Test Results

The acceptance criterion for the simulated equivalent thermal conductivity will be a deviation less than 25 percent of the experimental data.

5.1.4 Test Results

For the first set of test cases, the medium grid level is used. Grids were clustered in the near-wall region to capture the boundary layer developed by the natural convection

currents. The problem was formulated in the 2D domain assuming the third dimension to be of unit length. Wall boundary conditions with constant temperatures are specified for both the inner and outer cylinder walls. For the transitional and turbulent flow test cases, a standard k- ϵ turbulence model is used. Standard wall functions were used in the near-wall region. The steady solution is obtained using the SIMPLE scheme for pressure velocity coupling with second-order discretization for the pressure, momentum, energy and turbulence equations. The experimental study reported turbulent eddies and fluctuating velocity for higher Rayleigh numbers, but in the present validation study, high fidelity techniques like Large Eddy Simulation are not used, because these fluctuating eddies will not have any significant impact on the heat transfer process.

The equivalent thermal conductivity is calculated for all three test cases with three different Rayleigh numbers. The results are shown in Table 5-4, which lists the computed Rayleigh numbers, corresponding experimental values, the computed value from FLUENT Version 6.3, and the percentage deviation of values of Version 12.3 with the experimental data as well as with the previous computation.

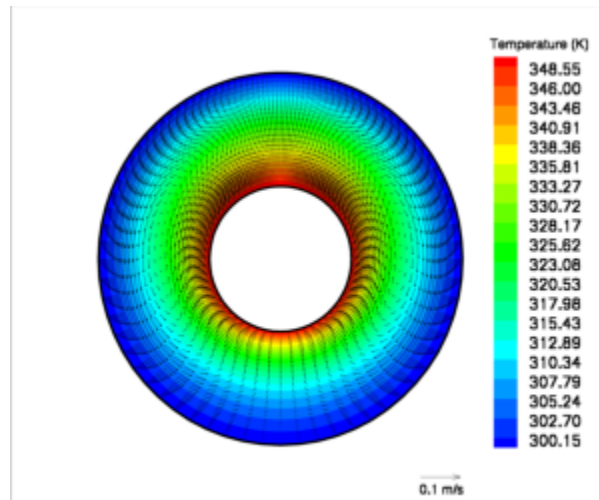
The equivalent thermal conductivity obtained from the grid independence study is highlighted in Table 5-5. With finer grid resolution, the percentage deviation from the experimental observation decreases, but the medium- and fine-grid solution produces an equivalent solution that is within the acceptable range of deviation from the experimental data. Hence, the medium-grid level was used for computational purposes to obtain computational economy without compromising accuracy.

Table 5-3 shows that all the values of equivalent thermal conductivity are within acceptable limits of deviation from the experimental data. For a Rayleigh number of 2.51×10^6 , the flow is in the transitional regime and it was treated as regular turbulent flow without any transition modeling.

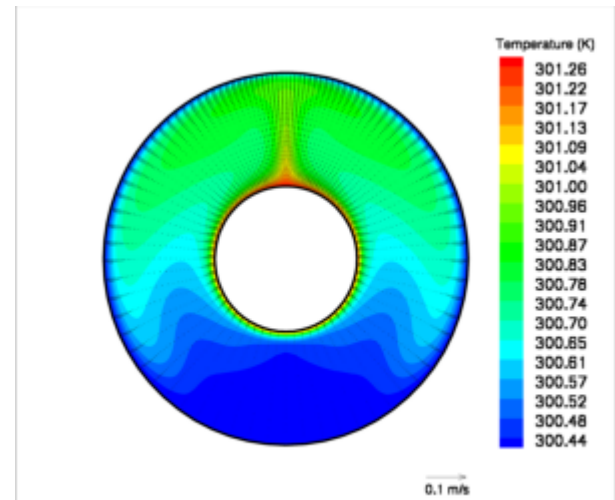
The general flow features of the validation case for all three Rayleigh numbers are highlighted in Figure 5-2, which shows that the flow pattern changes with increase in Rayleigh number. It can also be observed that the boundary layer at the inner and outer surface is well captured by FLUENT 6.3 especially for the laminar flow. For the transitional and turbulent flows, the boundary layer is not easily visible, because the plume of upward flow is stronger. This results in higher velocity near the wall. This result shows that the solver was able to reflect the change in physical parameters in the solution and effectively simulate turbulent natural convection.

Table 5-4. Comparison of Measured and Predicted Equivalent Thermal Conductivity for Concentric Cylinders					
Rayleigh Number	Experimental Value	Computed Value (Version 12.1)	Percent Deviation (from experiment)	Computed Value (Version 6.3)	Percent Deviation (from)
1.31×10^3	1.14	1.08	5.22	1.1	-3.5
2.51×10^6	7.88	7.80	0.95	8.02	1.77
6.60×10^7	18.65	18.75	-0.57	18.88	1.23

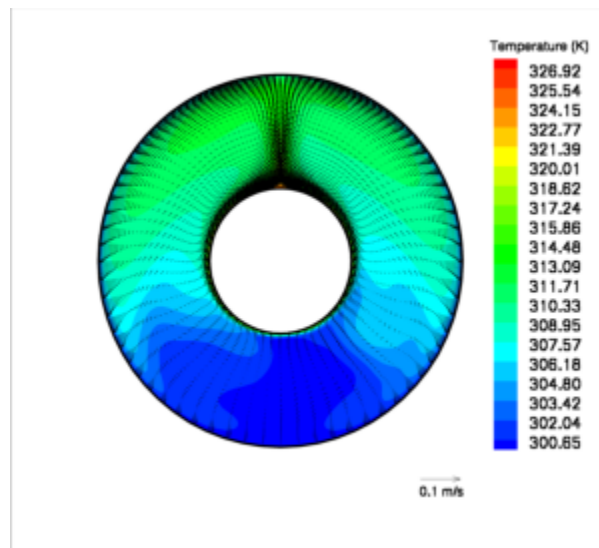
Table 5-5. Comparison of Measured and Predicted Equivalent Thermal for Three Grid Levels			
Grid Level	Experimental Value	Computed Value from Version 12.1	Percent Deviation
Coarse	1.14	1.20	5.2
Medium	1.14	1.10	-3.5
Fine	1.14	1.12	1.7



$Ra = 1.31 \times 10^3$



$Ra = 2.51 \times 10^6$



$Ra = 6.60 \times 10^7$

Figure 5-2. Velocity Vectors and Temperature Contours for Different Rayleigh Numbers

5.2 Natural Convection Along a Vertical Flat Plate

Natural convection along a flat, heated, vertical plate is one of the most basic flow configurations to test buoyancy-driven convection and is considered as a test case for validation of FLUENT. The analytical solution for this test case is available in Incropera and Dewitt (1996) for laminar boundary layers where the Rayleigh number is less than 10^6 . The analytical solution provides a local Nusselt number along the length of the vertical flat plate. The Nusselt number is a dimensionless temperature gradient at a surface and measures the efficiency of convection for heat transfer relative to conduction. The solution domain is shown in Figure 5-3.

5.2.1 Theoretical Basis

The analytical and empirical correlation for the heat transfer coefficient and Nusselt number variation along the vertical flat plate is provided in Incropera and DeWitt (1996). Ostrach (1953) numerically determined the Prandtl number dependence of the correlation and specific values of the Nusselt number for selected values of Prandtl

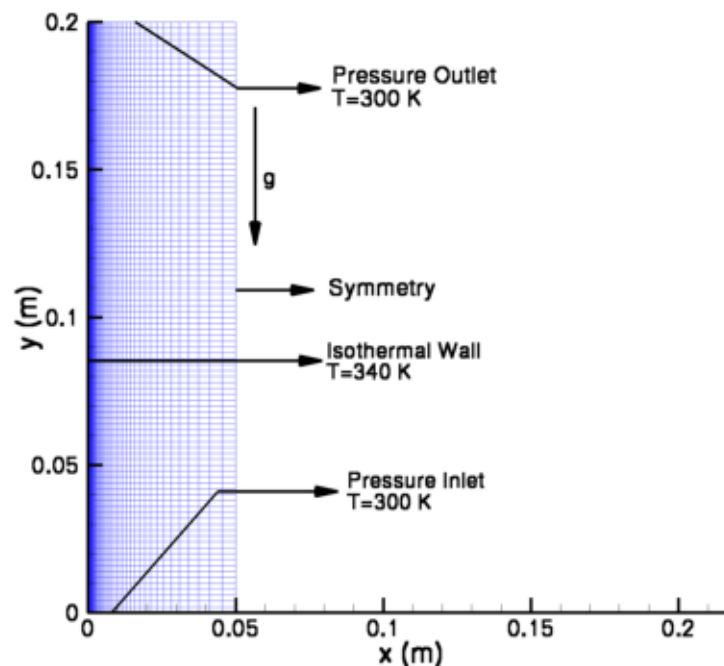


Figure 5-3. Computational Domain and Grid for Natural Convection Over Vertical Heated Plate

numbers. Later, LeFevre (1956) correlated these results by an interpolation formula to provide the Nusselt number in terms of Prandtl number and Grashof number

$$Nu(z) = \frac{0.75 Pr^{0.7}}{(0.609 + 1.221 Pr^{0.5} + 1.238 Pr)} \left(\frac{Gr(z)}{4} \right)^{0.25} \quad (5-3)$$

where

$Nu(z)$ — Local Nusselt number
 Pr — Fluid Prandtl number
 $Gr(z)$ — Local Grashof number

The Grashof number can be expressed as

$$Gr(z) = \frac{g \beta z^3 (T_s - T_f)}{\nu^2} \quad (5-4)$$

where

β — Thermal expansion coefficient of gas (1/K)
 ν — Kinematic viscosity of the gas in the annulus (m²/s)
 T_s — Wall surface temperature (K)
 T_f — Fluid temperature (K)
 g — Acceleration due to gravity (m/s²)
 z — Vertical distance

5.2.2 Test Input

FLUENT mesh and case files (*.msh and *.cas) are developed to model the vertical flat plate natural convection. The model is developed with an isothermal vertical wall with a temperature of 340 K. The standard properties of air at 300 K available from the FLUENT database are used in the simulation. The case is modeled as a 2D laminar incompressible flow problem with gravity as the body force and the Boussinesq approximation to capture the thermal buoyancy effects. Input and results for the test cases are on the attached media in the directory named natconv-12.1/.

The input parameters for the test case follow.

β — 0.0033 1/K
 T_s — 340 K
 T_f — 300 K
 Pr — 0.7
 L — 0.2 m

5.2.3 Expected Test Results

For the test result to be acceptable, computed Nusselt number distribution along the wall should be within 10 percent of the analytical solution. In general computation and measurement of Nusselt numbers, there is a higher degree of uncertainty (Incropera and DeWitt, 1996). Hence, matching of a computed Nusselt number within 10 percent could be considered sufficient condition acceptance. In addition, the computed flow field should qualitatively agree with the general understanding of the flow physics expected for natural convection flows along heated walls (Incropera and DeWitt, 1996; Ozisik, 1977).

5.2.4 Test Results

The test performed is analogous to that used to validate FLUENT Version 6.3 (Das and Basu 2008). The grid generated in the previous study was adopted in Version 12.1. The analytical values of the Nusselt number along the vertical plate were computed using the “custom field functions” option available in FLUENT so that a comparative study could be done. The postprocessing of the solution was done using the visualization software Tecplot-360. The analytical solution and computed solution for the Nusselt number was exported from FLUENT and postprocessed in Tecplot-360.

The validation test case described previously was solved using FLUENT as a 2D steady laminar flow problem. The heat transfer module of the FLUENT solver was enabled. The operating pressure of the domain was the specified 10132.5 Pa used elsewhere. At the heated wall, an isothermal boundary condition was used. At the bottom and top of the domain, a pressure inlet and outlet condition were specified. A symmetry boundary condition was imposed on the right end of the domain. Both the flow and energy equations were solved using the SIMPLE algorithm for pressure-velocity coupling. The PRESTO! Scheme was used to discretize the pressure equations, and the momentum as well as the energy equations used a second order upwind scheme for spatial discretization. Boussinesq approximation was used for density evaluation. The Boussinesq approximation neglects the effect of fluid-density dependence on pressure of the air phase, but includes the density dependence on temperature. It enables the flow to be treated as incompressible flow but still accounts for density variation locally in the momentum and energy equations. As the Rayleigh number of the flow will be less than the critical value, no turbulence models were used in the solution.

Figure 5-4 (a) shows the flow field simulated by the solver. The boundary layer profile and the velocity vectors are similar to those obtained from the previous validation study. The section AA shown in the figure is the cross section, where the exit velocity and temperature profile will be shown in Figure 5-6. Figure 5-4 shows that the boundary layer generated by the convective flow is well captured. The velocity vectors are shown for every other node for increased clarity. A zoomed section near the exit of the plate is highlighted in Figure 5-4 (b) for a better understanding of the boundary layer development. Both hydrodynamic and thermal boundary layers have developed due to the heated plate. The thermal boundary layer is shown by the colored contours, whereas the hydrodynamic boundary layer is illustrated by velocity vectors. As expected, both hydrodynamic and thermal boundary layer thicknesses increase as the flow moves vertically upward. This is consistent with the analytical solution (Incropera and DeWitt, 1996).

Figure 5-5 (a,b) compares the analytical Nusselt number along the vertical plate with computed results for Versions 12.1 and 6.3, respectively. The Nusselt number calculations were carried out using the custom field functions in FLUENT. The local Nusselt number increases monotonically for both the computed and analytical solution. The general trends are in good agreement with each other. The figure also shows two lines depicting the acceptable limits that are imposing the acceptance criteria on the analytical solution. It appears that the results predicted from Version 6.3 are slightly better than the newer version but both the results are within an acceptable limit. Therefore, the results of this test case are acceptable for software validation.

Figure 5-6 (a,b) shows the variation of the thermal and hydrodynamic boundary layers along the horizontal line A-A shown in Figure 5-5 for Versions 12.1 and 6.3, respectively. The patterns of these boundary layers are in agreement with those available in open literature (Incropera and DeWitt, 1996). The hydrodynamic boundary layer increases from a value of zero at the wall to a maximum value and then decreases to the free stream value of zero again. The thermal boundary layer has its maxima at the wall and then asymptotically decreases to the free stream value. These results indicate that the computed results satisfy the criteria of overall goodness and established understanding of the physical phenomena. There is a slight difference in results predicted for Version 12.1 as compared to 6.3.

Though the magnitude and velocity pattern matches, there is a slight difference in the velocity pattern. For Version 6.3, the velocity tapers off at the end of the domain, but for Version 12.1, it remains constant. These features, however, will not affect the near-wall region, where the buoyancy-driven flow plays a major role.

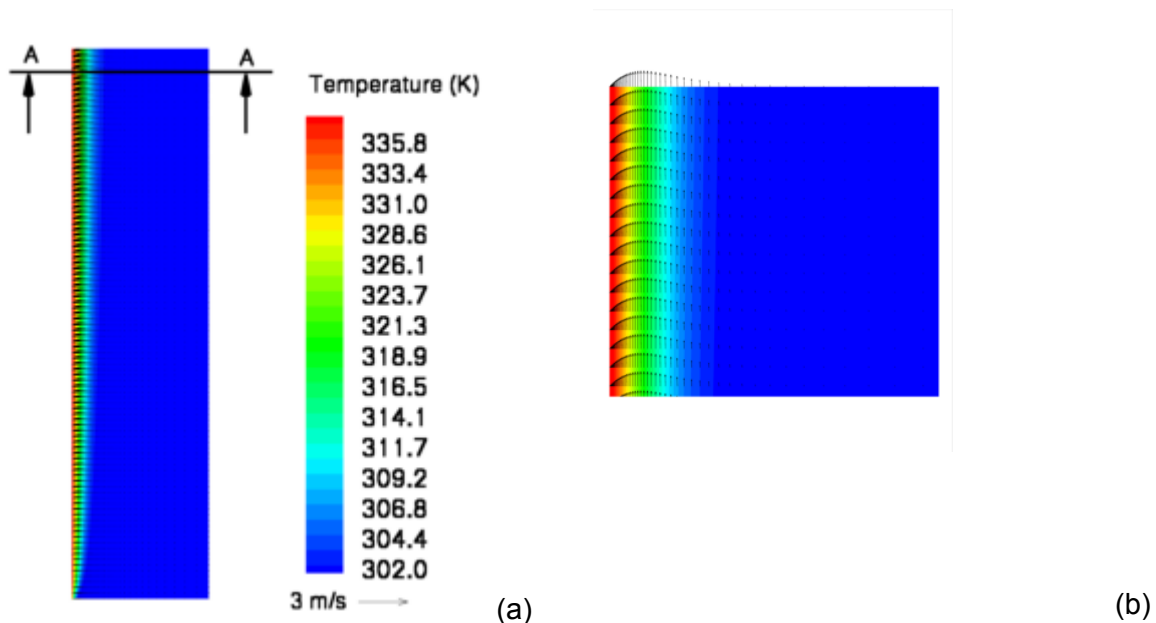
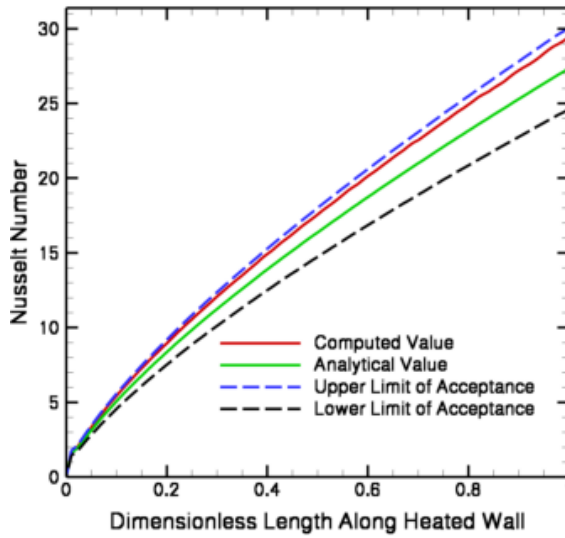
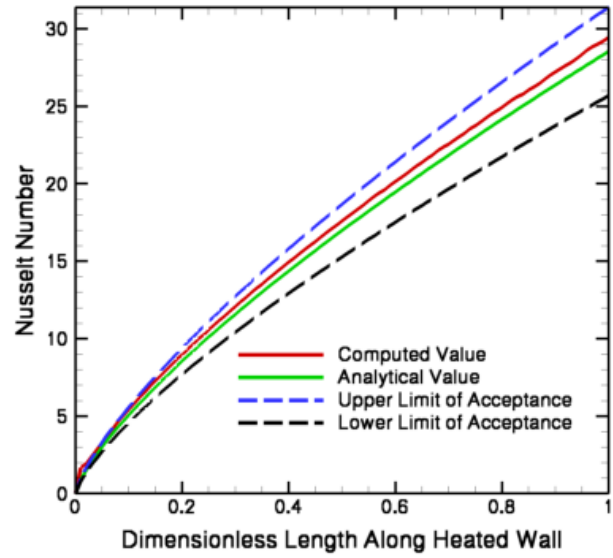


Figure 5-4 (a,b). Velocity Vectors and Temperature Contours (a) of the Domain and (b) Near the Exit

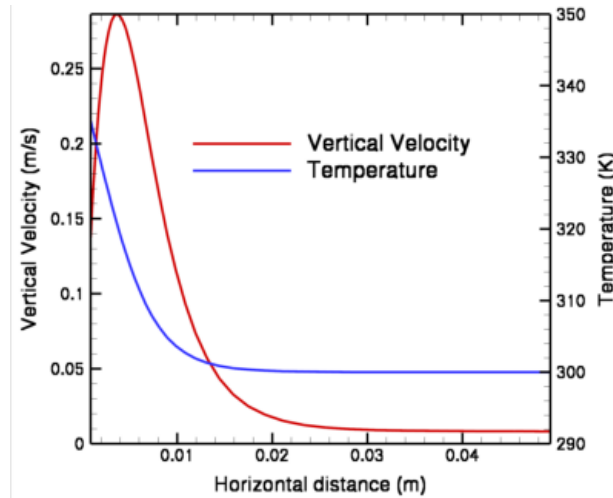


(a)

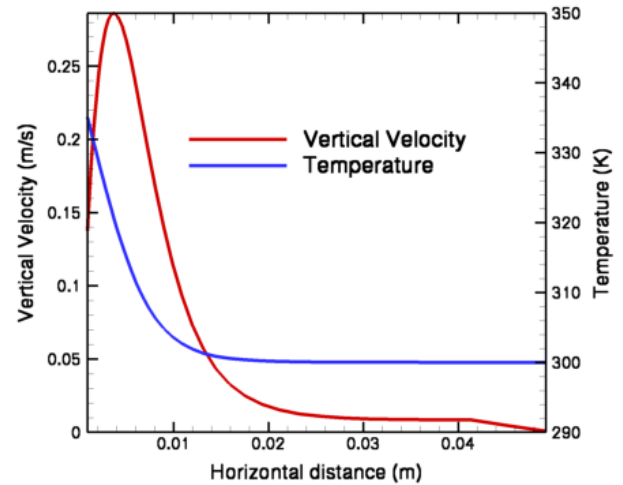


(b)

Figure 5-5 (a,b). Comparison of Computed and Analytical Values of Nusselt Number Where the Upper and Lower Limit of Acceptance is Within 10 Percent of Computed Value. (a) Version 12.1 and (b) Version 6.3



(a)



(b)

Figure 5-6 (a,b). Velocity and Temperature Distribution at the Plane A-A. (a) Version 12.1 and (b) Version 6.3

5.3 Flow Over Back-Facing Step

Driver and Seegmiller (1985) conducted experiments for incompressible turbulent flow over a rearward-facing step in a diverging channel flow. They measured mean velocities, Reynolds stresses, and triple products using a laser Doppler velocimeter. Skin friction coefficient distribution, pressure coefficient distribution along the floor, eddy viscosities, production, convection, turbulent diffusion, and dissipation (balance of kinetic energy equation) terms are extracted from the data. The present validation study is similar to that conducted for Version 6.3, and the skin friction and pressure coefficient

measurement from the experimental study will be used for FLUENT validation. The computed reattachment point of the flow downstream of the step will also be compared with experimental data.

Figure 5-7 shows the computational domain of the problem that mimics the experimental setup of Driver and Seegmiller (1985). The step height (H) is 0.0127 m and the expansion ratio is 1.125. The inlet computational domain is placed $4H$ upstream of the step, and the outlet is placed $40H$ downstream of the step. The upper end of the computational domain is placed at a distance of $9H$ from the bottom wall. The computational mesh and boundary conditions used in the simulation are also highlighted in Figure 5-7. Grid points are clustered at locations where a steep gradient of flow quantities is expected and in the near-wall region to capture the boundary layer. The dimensionless turbulent wall coordinate y^+ of 5 was used to obtain good resolution of flow features near the wall. The distance of the inlet plane from the step was not long enough to establish a turbulent boundary layer profile. As a result, approximate profiles of velocity, turbulent kinetic energy, and dissipation rates obtained from analytical solution were specified at the inlet to simulate a developed turbulent boundary layer. A pressure outlet boundary condition was used at the exit, and no-slip adiabatic conditions were specified at the wall boundary.

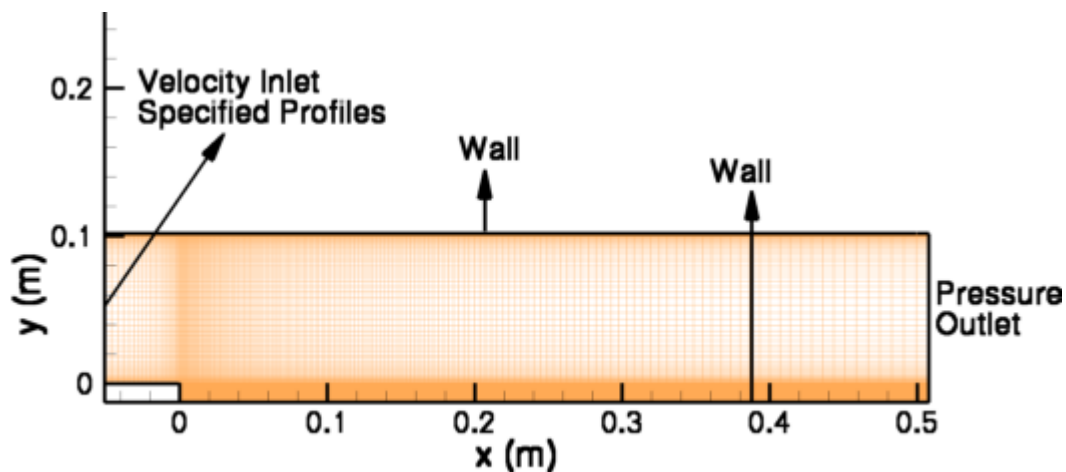


Figure 5-7. Computational Domain, Grid, and Boundary Conditions for Back-Facing Step

5.3.1 Theoretical Basis

Table 5-6 lists the flow parameters that Driver and Seegmiller (1985) used and that were adopted for the present validation study.

Table 5-6. Flow Parameters for Flow Over a Back-Facing Step	
Parameter	Value
Centerline velocity	44.2 m/s
Kinematic viscosity of air	$1.5 \times 10^{-5} \text{ m}^2/\text{s}$
Density of air	1 kg/m^3

Based on these parameters, the Reynolds number based on the step height is 37,400. As mentioned in the previous section, approximate velocity, turbulent kinetic energy, and dissipation rate profiles were used at the flow inlet. These profiles were derived based on the one-seventh-power law (Schlichting, 1960), which is given by

$$u = U \left(\frac{y}{\delta} \right)^{1/7} \quad (5-5)$$

where

y	—	Normal distance from the wall (m)
u	—	Velocity at y (m/s)
U	—	Free stream velocity (m/s)
δ	—	Boundary layer thickness (m)

The boundary layer thickness at the lip of the step was assumed to be half of the step height. The distributions of turbulent kinetic energy and dissipation at the inlet were approximated by profiles similar to the results of fully developed channel flow simulations.

Numerical results computed from the simulation were compared with the experimental data of Driver and Seegmiller (1985) for the bottom wall skin friction and static pressure coefficients. The skin friction coefficient is given by

$$C_f = \frac{\tau_w}{\frac{1}{2} \rho U^2} \quad (5-6)$$

where

τ_w	—	Shear stress at wall (Pa)
U	—	Free stream velocity (m/s)
ρ	—	Density of air (kg/m ³)

The pressure coefficient is given as

$$C_p = \frac{P_w - P_{fs}}{\frac{1}{2} \rho U^2} \quad (5-7)$$

where

P_w	—	Wall pressure (Pa)
P_{fs}	—	Free stream pressure (Pa)

5.3.2 Test Input

The input file used for the Version 6.3 validation study is used here. The model development intends to mimic the physical experiment Driver and Seegmiller (1985) conducted, and simulation parameters for the computation are selected to closely match the experimental conditions. The centerline velocity is set at 44.2 m/s, and air at 300 K is used as the working fluid to have a flow Reynolds number of 37,400. This test case is modeled in a 2D domain as turbulent incompressible flow and solved using the pressure-based incompressible Navier-Stokes equations without energy equation. Turbulence is simulated using a standard k- ω model with shear flow corrections. Domain size, grid, and boundary conditions are detailed in Section 5.3. The SIMPLEC algorithm is used for pressure-velocity coupling. Second-order upwind schemes are used for spatial discretization of momentum and turbulent transport equations. Input and results for this test case are on the attached media in the directory named /bfs-12.1/.

5.3.3 Expected Test Results

The acceptance criterion for the simulated equivalent thermal conductivity will be a deviation less than 25 percent of the experimental data.

Computed pressure and skin friction coefficient distribution will be compared with experimental observation for overall goodness of fit and visual matching. There should be a visual similarity between the computed and experimental results in terms of general trend, inflection, and curvature. The maximum deviation of the computed result from the experimental data at any point should not exceed 20 percent of the overall range of the parameter.

The location of the computed reattachment point downstream of the step height will also be compared against experimental results. As the flow separates from the step, it creates a circulating eddy and then gets attached to the bottom wall. The predicted reattachment location should be within 20 percent of the experimental observation.

5.3.4 Test Results

Figure 5-8 (a,b) shows the x-velocity contours near the vicinity of the back-facing step for Versions 12.1 and 6.3, respectively. For both the test runs, a vortex forms as the flow separates just downstream of the step. The flow subsequently reattaches to the wall after a certain distance away from the step. The figure shows that FLUENT was able to qualitatively capture the basic flow features described in the experimental work of Driver and Seegmiller (1985). The quantitative comparisons will be made later in this chapter. The figure also highlights the formation of boundary layers characterized by lower velocities in the lower and upper wall of the domain.

Likewise, Figure 5-9 (a,b) shows the distribution of turbulent kinetic energy around the step for Versions 12.1 and 6.3, respectively. As can be seen, the kinetic energy patterns are very similar and both follow the pattern observed in the experiment. There are some minor differences in pattern at the end of flow domain between the simulated cases that can be attributed to localized truncation error effect.

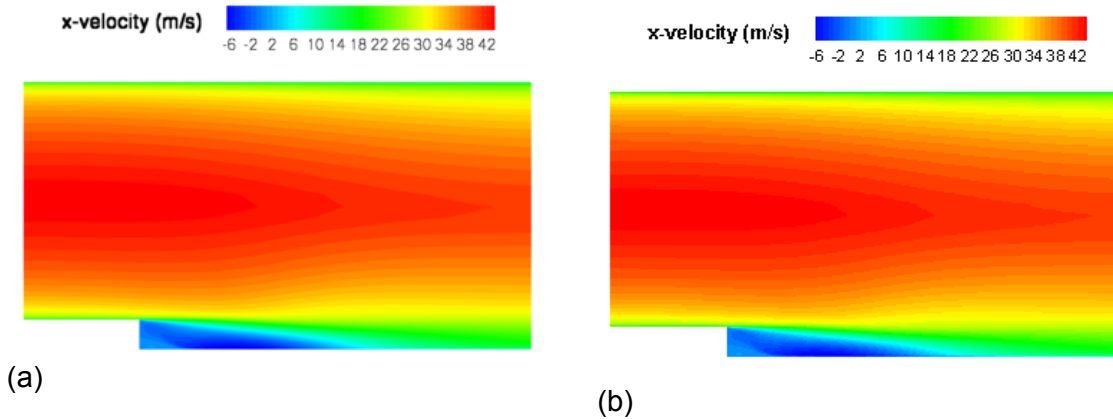


Figure 5-8 (a,b). Velocity Near the Vicinity of the Back-Facing Step. (a) Version 12.1 and (b) Version 6.3

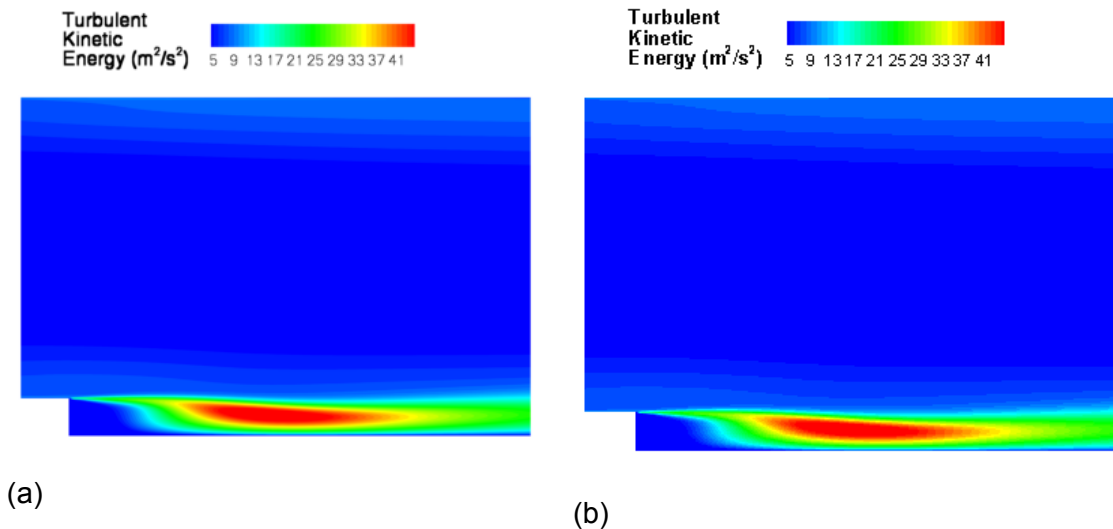


Figure 5-9 (a,b). Turbulent Kinetic Energy Near the Vicinity of the Back-Facing Step. (a) Version 12.1 and (b) Version 6.3

Figure 5-10 (a,b) compares the computed skin friction coefficient values with the experimental data along the floor downstream of the step for Versions 12.1 and 6.3, respectively. Both the computed and experimental data exhibit similar patterns and show almost identical trends. For both experimental values and computed data, the skin friction coefficient rapidly decreases just downstream of the cavity and subsequently increases before it asymptotically converges to a constant value. The maximum deviation of the computed results is within 6 percent of the experimental data and lies within the acceptable limit of the test condition of 20 percent deviation.

Figure 5-11 (a and b) shows the comparison of pressure coefficient values between the experimental and computed data for Versions 12.1 and 6.3, respectively. Like Figure 5-10 (a and b), a general qualitative agreement between the experimental and computed data can be seen because the data follow the same pattern and curvature for both cases. The two versions of FLUENT also provide nearly identical results. The maximum deviation of the computed results from the experimental observation is within 12 percent—within the acceptable limit of deviation.

As indicated in Figures 5-10 and 5-11, the computed and experimental reattachment points are approximately determined from the results. The reattachment points are defined at locations where the pressure coefficient or skin friction coefficients recover from abrupt change and follow a nearly constant value. The simulated reattachment occurred at a $4.07H$ distance downstream of the step, and the experimental data show the reattachment point at $3.7H$. This means that computed results overpredict the location by 10 percent of the experimental value, but this deviation is within acceptable limits of the validation tests. In addition, predicting the reattachment point is difficult using a numerical tool and FLUENT has provided a reasonably good result for the reattachment location.

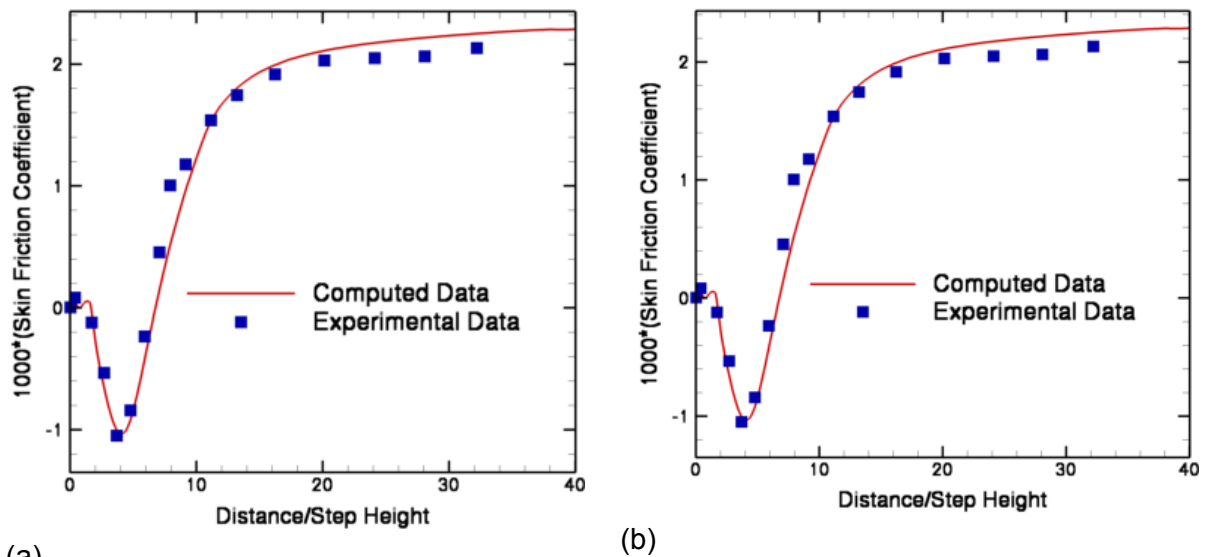


Figure 5-10 (a,b). Comparison of Computed Skin Friction Coefficient With Experimental Data. (a) Version 12.1 and (b) Version 6.3

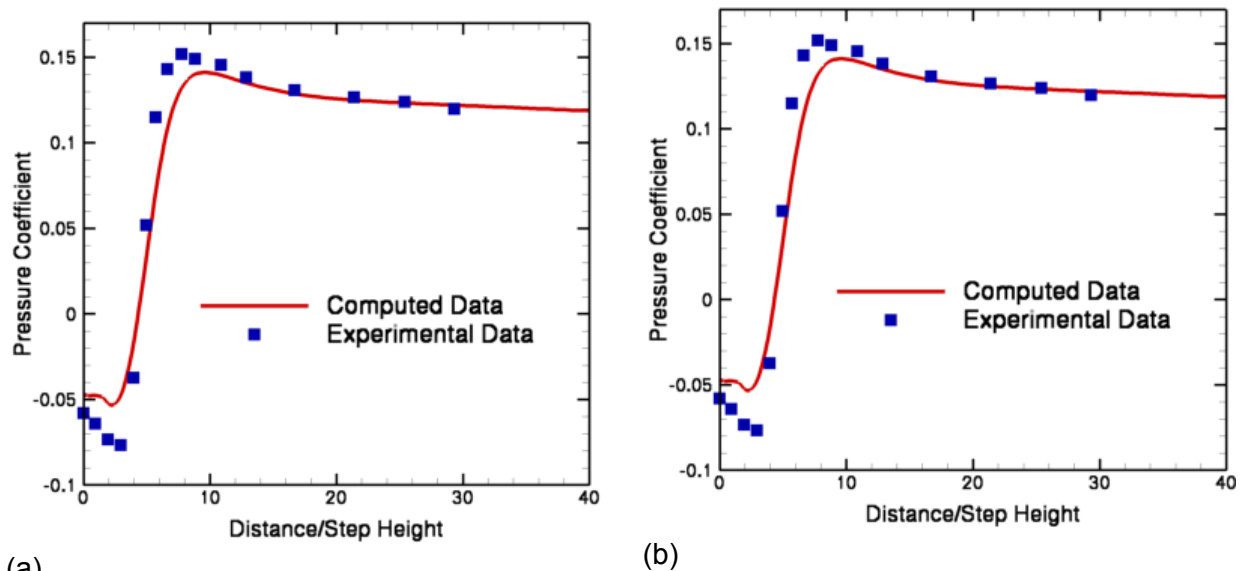


Figure 5-11 (a,b). Comparison of Computed Pressure Coefficient With Experimental Data. (a) Version 12.1 and (b) Version 6.3

5.4 Flow and Heat Transfer Over Expansion Pipe

The test case of flow and heat transfer over an expansion pipe is selected to validate the capability of FLUENT. The test case numerically replicates the experiment Baughn, et al. (1984) conducted that provides a good benchmark to validate forced convection and heat transfer. The experimental study measured the local heat transfer coefficient downstream of an abrupt expansion in a symmetric, circular channel with a constant heat flux applied to the wall.

A constant heat flux of 0.3 W/m^2 was imposed on the pipe wall for the expanded larger pipe, whereas an adiabatic boundary condition with zero heat flux was used as the pipe boundary for the smaller pipe.

The computational domain of the validation test case is shown in Figure 5-12. The domain geometry, flow, and boundary conditions are selected to accurately replicate the experimental setup and test conditions. The 2D solution domain covers only half of the pipe, taking advantage of the symmetry. The inlet is placed 1 m upstream of the expansion step, which is shown as H in the figure. The expansion ratio d/D of 0.4 with an entry diameter of $d = 1.33 \text{ m}$ is used. The downstream boundary is placed at a distance of $40H$ from the step. Grids are clustered near the wall and the step to capture the steep gradient of flow quantities in these regions. Suitable profiles of velocity and turbulent quantities were specified at a velocity inlet. At the exit, a pressure outlet was specified.

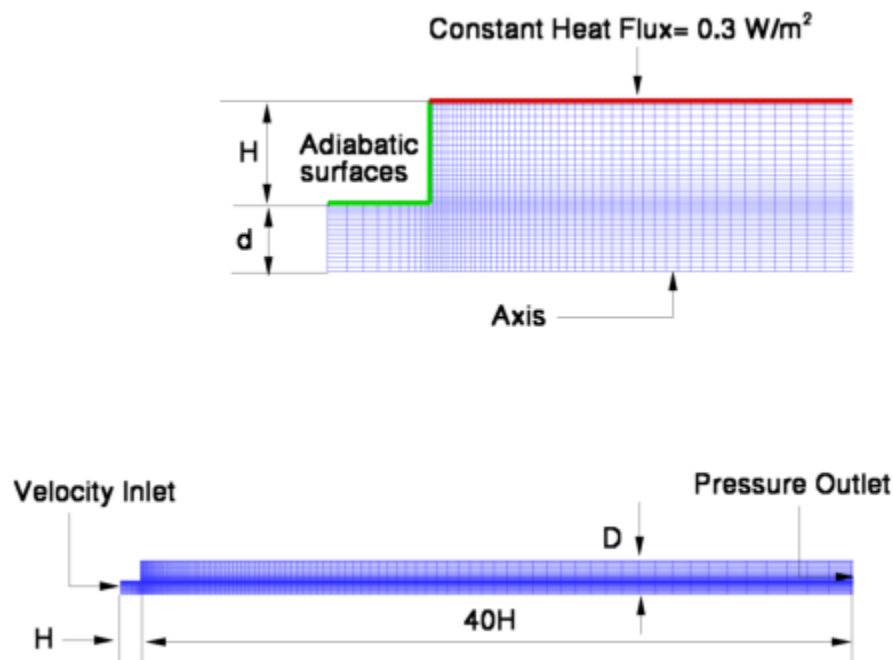


Figure 5-12. Computational Domain Grid and Boundary Conditions for Flow and Heat Transfer Over Expanded Pipe

5.4.1 Theoretical Basis

The heat transfer coefficient obtained from the Baughn, et al. (1984) experiment is presented in terms of Nusselt number ratios along the heated wall of the larger pipe. The Nusselt number for internal flows is calculated based on bulk temperatures. The relevant quantities required to calculate bulk temperature and Nusselt numbers are described here.

The bulk temperature is given by

$$T_B(x) = \frac{\dot{q}''(x)4x}{Re \mu c_p} + 273 \quad (5-8)$$

where

$\dot{q}''(x)$	—	Local heat flux (W/m ²)
Re	—	Flow Reynolds number
c_p	—	Fluid-specific heat (J/kg-K)
x	—	Distance (m)

The local Nusselt number is given as

$$Nu(x) = \frac{\dot{q}''(x)D}{\{T_{wall}(x) - T_B(x)\}k} \quad (5-9)$$

where

$T_{wall}(x)$	—	Local wall temperature (K)
k	—	Fluid thermal conductivity (J/m-K)

The experimental results are provided in terms of the ratio of the local Nusselt number and the Dittus-Boelter correlated Nusselt number (Todreas and Kazimi, 1990). The Dittus-Boelter correlation is given by

$$Nu_{DB} = 0.023 Re^{0.8} Pr^{0.4} \quad (5-10)$$

where

Pr	—	Flow Prandtl number = 0.7 for the present simulations
----	---	---

5.4.2 Test Input

The proposed test is one of the standard documented validation studies of FLUENT (Fluent Inc., 2007a,c). The grid and case file available from the validation repository are used for the study (Fluent Inc., 2007b). Test input parameters are selected to match the simulation conditions with experimental setup and conditions. The grid, domain, and

boundary conditions related to the test case were already discussed in Section 5.4. The problem was modeled in an axisymmetric domain, and the incompressible Navier-Stokes equations are solved in conjunction with the energy equations. A standard $k-\epsilon$ turbulence model with standard wall functions is used to simulate turbulence. Air properties used in the simulation are obtained from the FLUENT database. The SIMPLE algorithm is used to couple pressure and velocity. For spatial discretization, a second-order upwind scheme is used for the momentum and turbulence equations. At the inlet, profiles of fully developed axial and radial velocities as well as profiles for turbulent kinetic energy and dissipation are used. Input and results for the test cases are on the attached media in the directory named /exp-pipe-12.1/.

5.4.3 Expected Test Results

The computed Nusselt number ratio (Nu/Nu^{DB}) will be compared with the experimental data Baughn, et al. (1984) provided. The predicted distribution will be compared with experimental observations for overall goodness of fit and visual matching. There should be a visual similarity between the computed and experimental results in terms of general trend, inflection, and curvature. The maximum deviation of the computed result from the experimental data at any point should not exceed 20 percent of the overall range of the parameter. The general features of the flow field should also be in qualitative agreement with the current understanding of internal flows and expansion pipes.

5.4.4 Test Results

For this specific study, simulated results using FLUENT Version 12.1 are presented. Figure 5-13 shows the velocity, temperature, and turbulent kinetic energy distribution of the flow field. There is a separation region in the velocity field immediately after the constriction. The temperature distribution shows elevated temperature in the near-wall region. The turbulent kinetic energy shows the mixing pattern that follows the sudden expansion. These behaviors are in qualitative agreement with the experimental observation (Baughn, et al., 1984) and are almost identical to the calculated turbulent kinetic energy contours obtained using FLUENT Version 6.3.

Figure 5-14 shows the comparison of experimental Nu/Nu_{DB} to the computed solutions along the heated wall. The computed and experimental data exhibit similar patterns and trends. The distribution increases steadily to reach a peak value 10 m from the step and then decreases asymptotically. In general, the computed results overpredict the Nusselt number. However, the maximum deviation from the experimental data does not exceed 6.9 percent, which is within acceptable range as stated in Section 5.4.4.

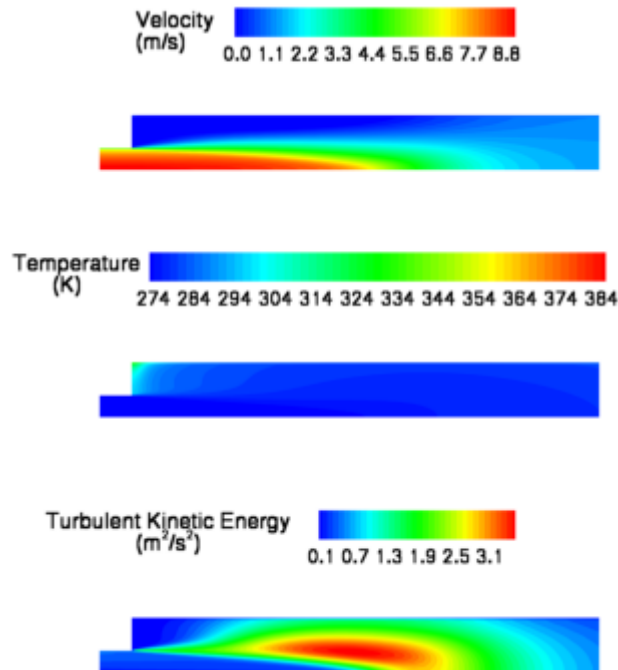


Figure 5-13. Velocity, Temperature, and Turbulent Kinetic Energy in the Flow Field Using Version 12.1

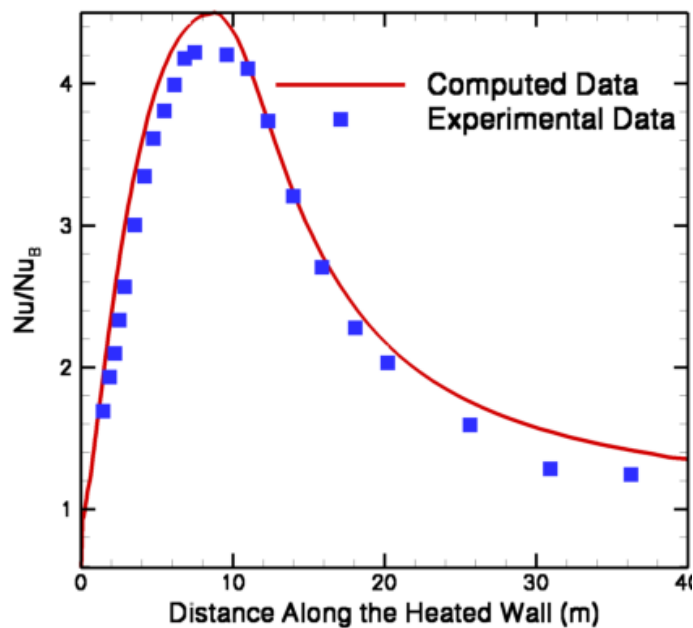


Figure 5-14. Comparison of Experimental and Computed Nu/Nu_{DB} Along the Heated Wall

6 HIGH SPEED FLOWS

The test cases described in this section validate the FLUENT code for application in high speed flows. Unlike the tests related to heat transfer and multiphase flows, all the test cases for high speed flows use the density-based solver of FLUENT, which is meant for simulating compressible flows.

6.1 Flow Over Wedge

An analytical solution of supersonic flow over a wedge provides a method to validate the accuracy of FLUENT for high speed compressible flows. The test assumes an isentropic flow of ideal compressible gas.

The flow physics of the test case are shown in Figure 6-1. The high speed supersonic flow contacts the leading edge of the ramp and generates an oblique shock at an angle β as shown in the schematic.

The flow properties and parameters across the shock exhibit a sharp discontinuity. The flow features and analytical treatment are detailed in Anderson (1984). The present validation study will focus on validating the capability of FLUENT in predicting the general compressible flow features and capturing the flow properties across the shock.

Figure 6-2 shows the domain, grid, and boundary conditions of the test case for Version 12.1 that are identical to those used in validating FLUENT Version 6.3. The wedge angle for the test geometry is 15° , with an inlet Mach number of 2.45. These conditions will produce an oblique shock at an angle of 38° and an exit Mach number of 1.8. At the inlet, the total and static pressure are specified and produce a Mach 2.45 stream. At the outlet, pressure outlet conditions are specified. The present test case considered inviscid flow because the objective was to assess the capability of FLUENT in capturing characteristic features of high speed flow like shock and discontinuity across the shock. Intricate details of compressible boundary layer development and shock boundary-layer interaction were not considered in the study. Hence, at the bottom wall,

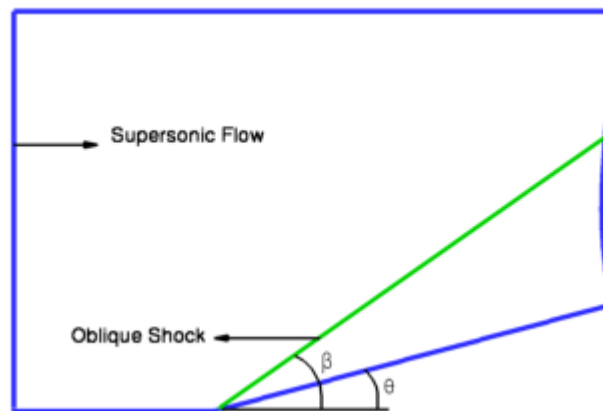


Figure 6-1. Features of Supersonic Flows Over Wedge

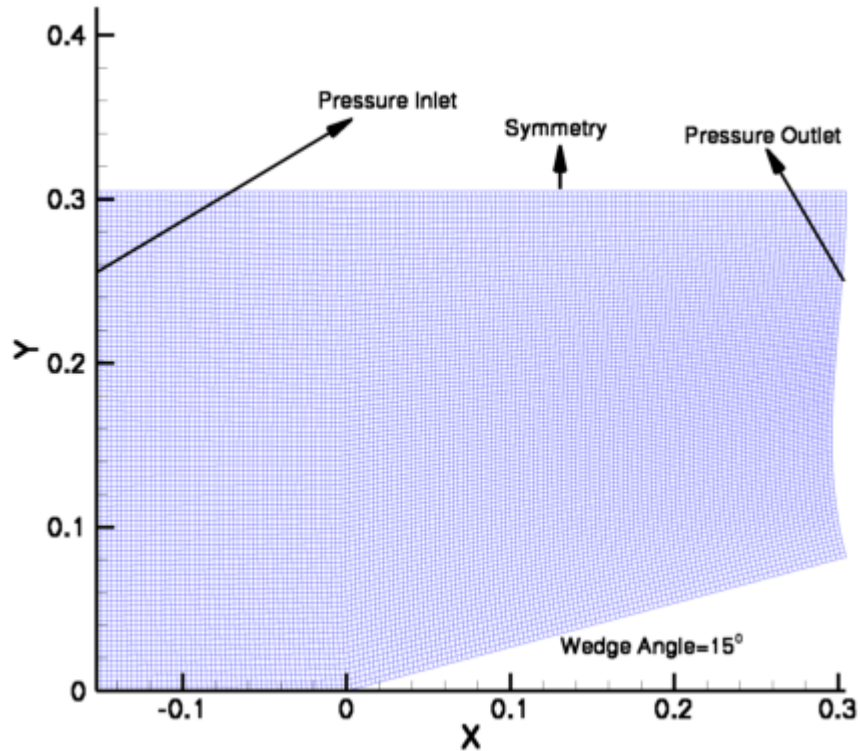


Figure 6-2. Domain, Grid, and Boundary Conditions for Flow Over Wedge

slip boundary conditions are specified. A symmetry boundary condition is imposed at the upper plane of the domain. Uniform grid spacing is used throughout the computational domain, and unlike the previous test cases, grids were not clustered in the vicinity of the wall, because there will be no velocity gradient without viscous forces. The grid and flow conditions used in the present validation test are obtained from a similar study using the NPARC-WIND flow solver (Bush, et al., 1998; Georgiadis, et al., 2006).

6.1.1 Theoretical Basis

The analytical solution for the present validation case is documented in open literature (Anderson, 1984). The principal flow quantities of interest are the ratio of the Mach number and other flow parameters such as density and temperature across the shock.

The Mach number ratio across the shock is given by

$$\frac{M_2}{M_1} = \frac{\sin \beta}{\sin(\beta - \theta)} \quad (6-1)$$

where

M_1	—	Inlet Mach number
M_2	—	Mach number after the shock
β	—	Shock angle
θ	—	Wedge angle

The shock angle β is computed from the following relationship

$$\tan \theta = 2 \cot \beta \left[\frac{M_1^2 \sin^2 \beta - 1}{M_1^2 (\gamma + \cos 2\beta) + 2} \right] \quad (6-2)$$

where

γ	—	Ratio of specific heat = 1.4
----------	---	------------------------------

The dependent quantity β has a transcendental relationship with the independent variable θ , and β cannot be determined using a direct algebraic relationship. As a result, Eq. (6-2) must be solved using a numerical technique to obtain the value of shock angle β .

The density ratio across the shock is given by

$$\frac{\rho_2}{\rho_1} = \frac{(\gamma + 1)M_1^2 \sin^2 \beta}{(\gamma - 1)M_1^2 \sin^2 \beta + 2} \quad (6-3)$$

where

ρ_1	—	Inlet density
ρ_2	—	Density after shock

The ratio of other quantities like static temperature and pressure can be derived from Eqs. (6-1) through (6-3) and the ideal gas law for air.

6.1.2 Test Input

A hypothetical test case is constructed to replicate the flow problem shown in Figure 6-1. The grid, domain, and boundary conditions related to the test case were already discussed in Section 6.1. The problem is modeled in a 2D domain, and the density-averaged implicit compressible Navier-Stokes equations are solved in conjunction with the energy equations. The Green-Gauss cell-based gradient option is used in the solution. The convective flux terms are solved using a Roe scheme. A second order upwind scheme is used for spatial discretization. As mentioned previously, air was

treated as inviscid flow in the solution. Air properties used in the simulation are obtained from the FLUENT database. Input and results for the test case are on the attached media in the directory called /wedge-12-1/.

6.1.3 Expected Test Results

To acceptably simulate high speed flows, the flow solver should predict a flow field that is in qualitative agreement with the theoretical understanding of supersonic flow in ramps (Anderson, 1984). The computed flow field data should be able to capture the shock, and the computed shock angle should be within 10 percent of the value of analytical value. Mach number ratio across the shock will be compared against the analytical solution, and the computed values should lie within 20 percent of the analytical solution. Similarly, the predicted density ratio across the shock is expected to lie within 20 percent of the analytical value. The acceptance criteria are identical to those used in validating Version 6.3.

6.1.4 Test Results

As observed in any transonic flows, a sharp oblique shock is generated at any sharp corner on the ramp. Figure 6-3 illustrates this feature in the simulated density field of the domain. The flow field is in agreement with the general understanding of supersonic flow over wedges. The fluid density undergoes a sharp change across the shock and does not vary anywhere else, which is in agreement with the existing studies (Anderson, 1984). The shock angle for the computed solution was calculated from the flow field data. The analytical value of the shock angle is 37.56° , and the computed value obtained from FLUENT Version 12.1 is approximately 37.50° . Hence the deviation between computed and experimental data is approximately 0.156 percent and is well within the acceptable range as outlined in the previous section.

Figure 6-4 shows the pressure contour in the simulated flow field. It is analogous to the density field and creates the same shock angle at the ramp. The numerical value of this angle is 37.50° , whereas the analytical value is 37.56° . The percentage difference is below 0.2 percent and lies within the acceptable limit.

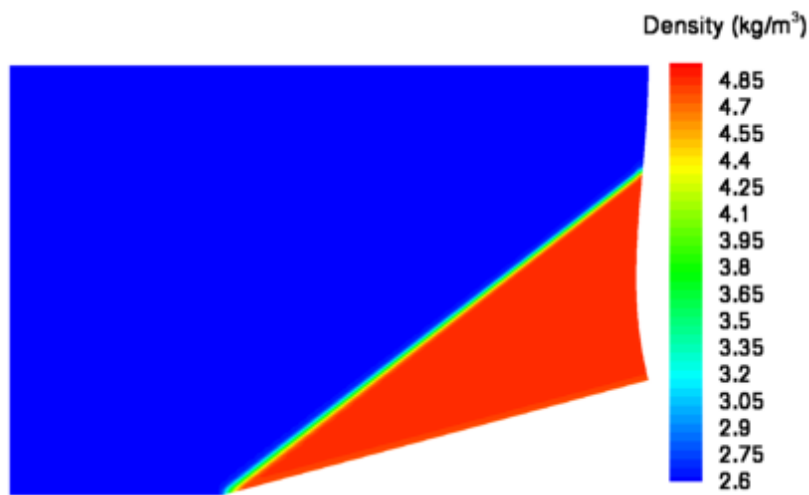


Figure 6-3. Simulated Density Field Using FLUENT Version 12.1

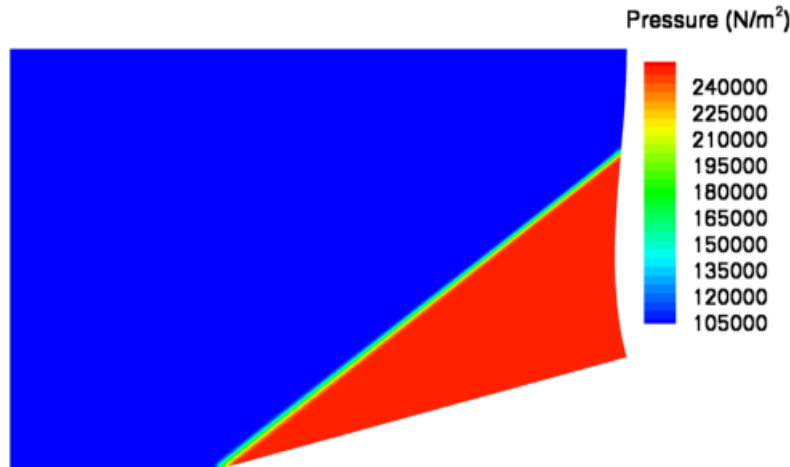


Figure 6-4. Simulated Pressure Field Using FLUENT Version 12.1

Figure 6-5 (a,b) shows the comparison of Mach number and density ratio (ρ_2/ρ_1) with analytical solution along the floor of the computational domain. These results are almost identical to those obtained using Version 6.3. Both these flow quantities encounter a sudden change across the shock. The simulated results match reasonably well with the analytical data. For the Mach number distribution, the maximum deviation of the computed result is well within 2.7 percent of the analytical solution. For the density distribution, the deviation between the analytical and computed solution is within 1.6 percent. Therefore, the computed results are in agreement with the analytical solution within the acceptable limits.

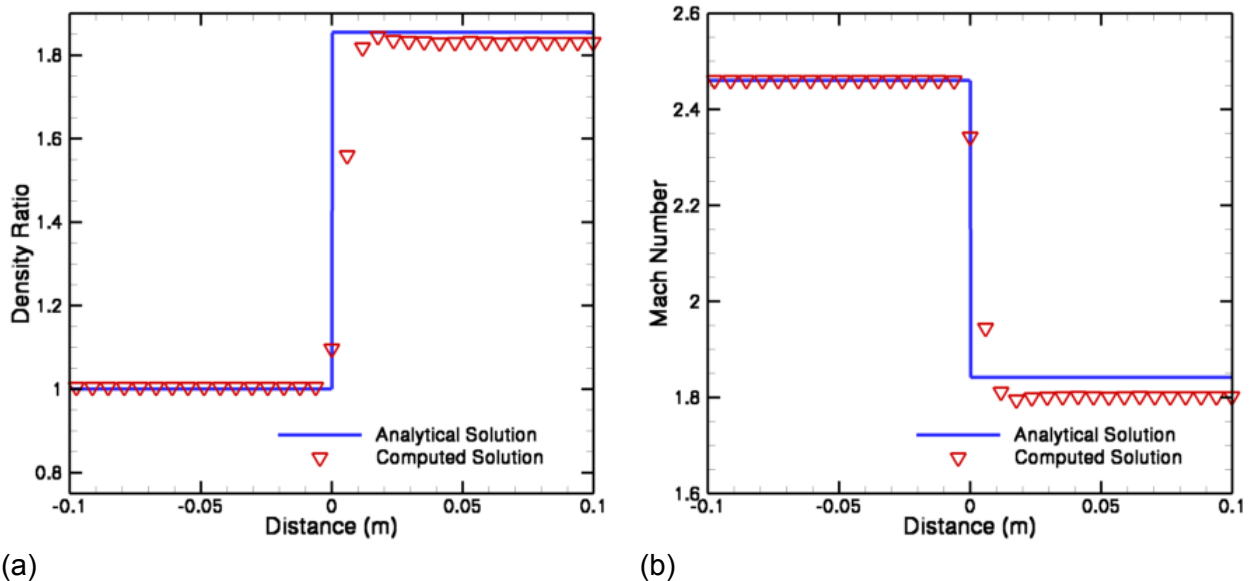


Figure 6-5 (a,b). Comparison of Analytical and Computed Solutions Along the Floor. (a) Mach Number and (b) Density Ratio

6.2. Turbulent Mixing Layer of Compressible Flow

Goebel and Dutton (1991) performed a detailed experimental study of the turbulent mixing layer, which is used as a validation benchmark for FLUENT for modeling viscous compressible turbulent flows. It is one of the tests documented in the validation archive of FLUENT (Fluent Inc., 2007a) and was also used to validate Version 6.3. The experimental investigation measured the turbulent kinetic energy and axial velocity profiles that are used to compare the simulated results in the present test case. In this test case, two fluid streams with different velocities are injected inside a rectangular channel. Due to the velocity gradient, a turbulent mixing process will start and continue as the flows travel downstream.

The computational domain and grid, along with boundary conditions, are shown in Figure 6-6. The length of the computational domain is chosen such that the local Reynolds number at the exit of the test section, based on the velocity difference between the streams and the mixing layer thickness, is greater than 10,000, which is needed for the complete development of the mixing layer. This is because the experimental study found that the development of the mixing layers required a Reynolds number (based on the free stream velocity difference and local mixing-layer thickness) on the order of 1×10^5 . Pressure inlet boundary conditions were separately specified for each incoming fluid. The inlet Mach numbers for the two fluid streams are 2.35 and 0.38. At the outlet, the gauge pressures are specified. Symmetry boundary conditions are used in the upper and lower wall, as resolving the near-wall flow field is not as important as resolving the mixing layer for this test.

6.2.1 Theoretical Basis

Goebel and Dutton (1991) investigated the compressible turbulent mixing layer by pressure measurements, Schlieren photographs, and velocity measurements with a two-component laser Doppler velocimeter system. They examined seven cross-sectional areas along the domain and found that in the fully developed regions of the mixing layers, transverse turbulence intensities and normalized kinematic Reynolds

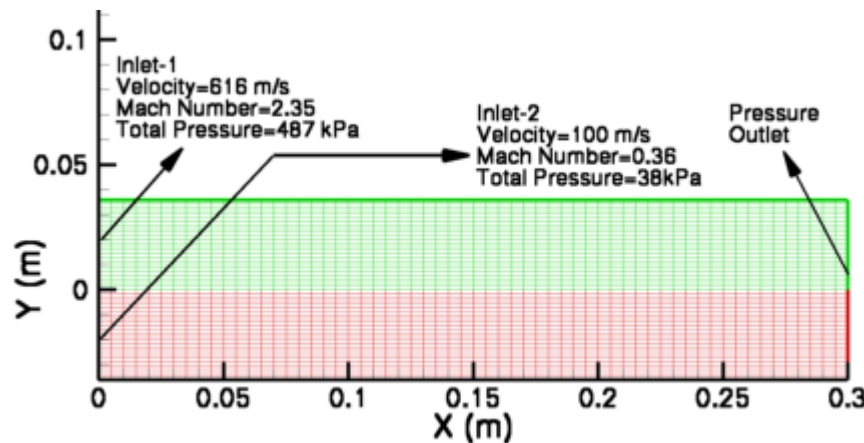


Figure 6-6. Computational Domain, Grid, and Boundary Conditions for Compressible Mixing Layer

stresses decrease with increasing relative Mach number. On the other hand, the streamwise turbulence intensities and kinematic Reynolds stress correlation coefficients remained relatively constant. The relative Mach numbers were computed based on the relative velocity between the two mixing streams.

6.2.2 Test Input

Mesh files available from the FLUENT validation repository are used for this study (Fluent Inc., 2007b). Inputs files that were used for validating FLUENT Version 6.3 are also used for the present study. Test input parameters in the case file (*.cas) were generated to match the simulation conditions with the experimental setup and conditions as Goebel and Dutton (1991) described. The grid, domain, and boundary conditions related to the test case were already discussed in Section 6.2. The problem is modeled in a 2D domain, and the density-averaged compressible Navier-Stokes equations are solved in conjunction with the energy equations. Turbulence is simulated using a standard k- ϵ turbulence model with standard wall functions. The convective flux terms are solved using a Roe scheme. A second-order upwind scheme is used for spatial discretization for the momentum and turbulence transport equations. Air properties used in the simulation are obtained from the FLUENT database. Input and results for the test case are on the attached media in the directory called /mixing-12.1/.

6.2.3 Expected Test Results

The computed turbulent kinetic energy and axial distribution 100 mm from the inlet will be compared with experimental data of Goebel and Dutton (1991). The predicted distribution will be compared with experimental observation for overall goodness of fit and a qualitative match. There should be a visual similarity between the computed and experimental results in terms of general trend, inflection, and curvature. The maximum deviation of the computed result from the experimental data at any point should not exceed 25 percent of the overall range of the parameter. The general features of the flow field should also be in qualitative agreement with the current understanding of mixing layer. The contours of turbulent kinetic energy and axial velocity should be able to qualitatively predict the mixing zone.

6.2.4 Test Results

Some marked differences were noticed when trying to use the FLUENT Version 6.3 files to validate the FLUENT Version 12.1 software. The original input file used multigrid technique to achieve faster convergence, with a Courant number of 3. The new version, however, diverged with that setup. As an alternative, a multigrid initialization with a low initial Courant number was specified that was gradually increased as the solution converged. From this exercise, it can be concluded that the convergence criteria for high speed flows are different for Versions 12.1 and 6.3.

Figure 6-7 shows the axial velocity in the computational domain; the mixing layer thickness gradually increases as the flow moves downstream. This is in agreement with the established understanding of mixing layer physics through various experimental and computational studies of mixing layers in splitter plates, exhaust nozzles, and cavities.

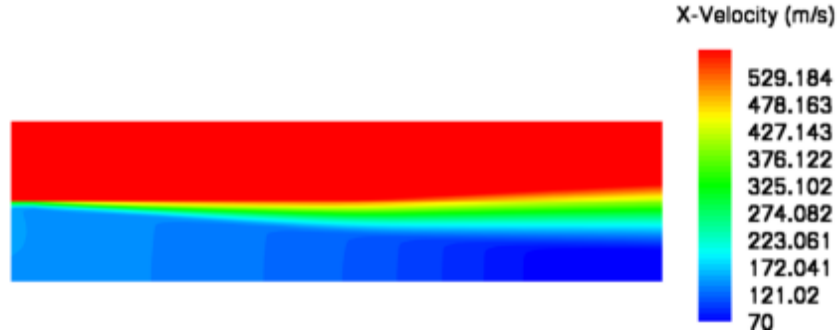


Figure 6-7. Velocity Distribution in the Mixing Layer

The figure also shows that the mixing layer achieves a developed stage near the end of the domain where the Reynolds number based on relative velocity is about 10^5 . Previous studies have indicated that the flow inside the mixing layer is usually unsteady in nature, but the present validation study employs the steady version of the Navier-Stokes solver as it is only necessary to obtain average flow field variables for comparison.

The turbulent kinetic energy distribution for the domain is shown in Figure 6-9. It highlights the same trend observed in Figure 6-7. The results are very similar to those obtained using Version 6.3. The mixing layer grows along the downstream direction, and the maximum value of turbulent kinetic energy is along the centerline of the flow where the velocity gradient is also maximum. Figures 6-7 and 6-8 highlight the fact that the flow solver captured the basic physical phenomena of fluid mixing.

Figure 6-9 shows the comparison of experimental turbulent kinetic energy to the computed solutions 100 mm from the inlet across the solution domain. The computed and experimental data exhibit similar patterns and trends. The distribution increases steadily to reach a peak value along the centerline of the domain and then decreases to its initial value. In general, the computed results underpredict the turbulent kinetic energy. The deviation is maximum near the centerline of the domain.

The predicted results show a vertical shift in comparison to the experimental data. As a result, the peak turbulent kinetic energy is predicted at a different height. This causes a higher deviation of computed values from experimental observation on the bottom half of the domain where the slope of kinetic energy is high. The deviation can be better

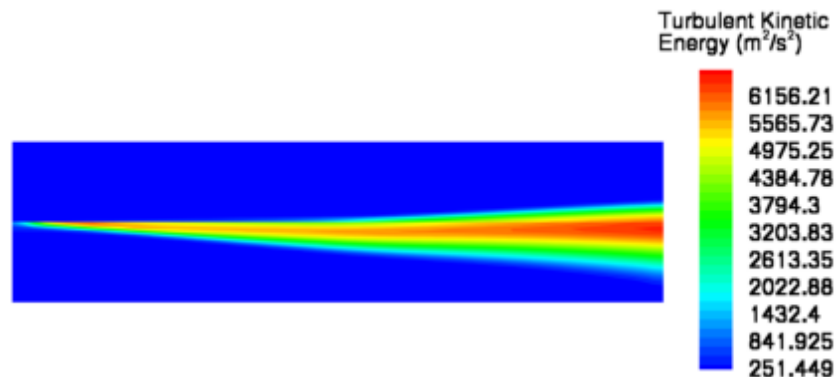


Figure 6-8. Turbulent Kinetic Energy Distribution in the Mixing Layer

estimated if the experimental data are compared with computed data at an equivalent location on the predicted turbulent kinetic energy curve.

Figure 6-10 compares experimental and computed axial velocity profiles at the same location. The profile shows that the simulation well captured the velocity gradient across the two fluids.

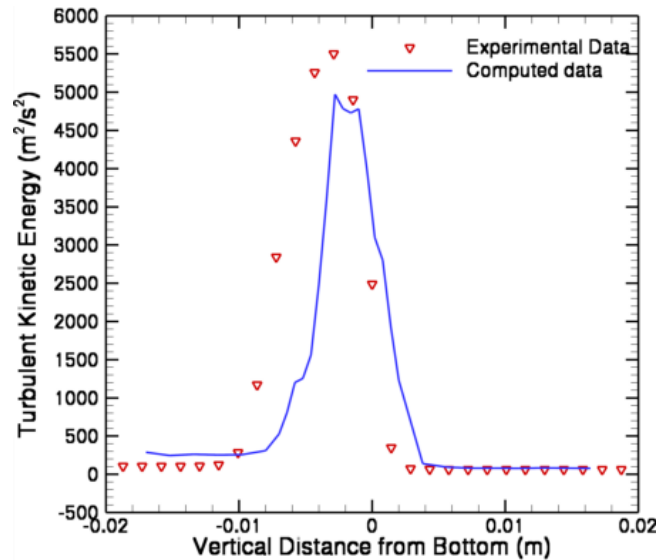


Figure 6-9. Comparison of Computed and Experimental Turbulent Kinetic Energy at $x = 100$ mm

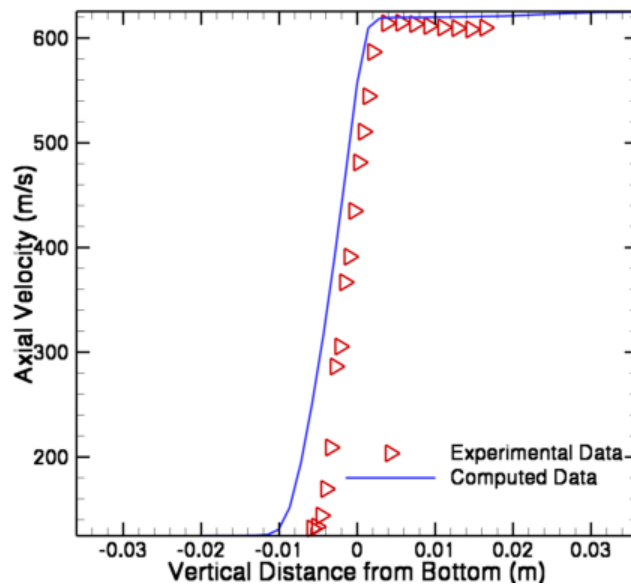


Figure 6-10. Comparison of Computed and Experimental Axial Velocity at $x = 100$ mm

The experimental and computed results show a good agreement in terms of trend, curvature, inflection, and overall goodness of fit. The maximum deviation occurs near the bottom of the domain because in the simulations, the effect of the bottom and top wall was neglected—as the main focus was to capture the mixing zone. The effect is greater on the bottom wall because, due to the lower velocity of the flow, the boundary layer is thicker compared to the upper wall. However, the deviation of the computed result is not more than 6 percent of the experimental data, which is within the range of deviation as per the validation requirement described in Section 7.2.3.

7 RADIATION HEAT TRANSFER

In this section, two test cases are presented for validation using the FLUENT code to model radiation heat transfer. These validation tests will only focus on surface radiation through nonparticipating, transparent, homogenous media. The convective flow between the surfaces was neglected. Radiation configuration factors or the view factors were calculated using the FLUENT solver and were not supplied externally.

7.1 Radiation Between Two Parallel Surfaces

A one-dimensional analytical solution of radiation heat transfer between two parallel plates provides a method to validate the accuracy of FLUENT for modeling the radiation process. To establish radiation heat transfer as the dominant mode of energy exchange between the two surfaces, this test assumes no convective flow in the gap. However, conduction heat transfer through the air gap will take place but will have a minor contribution to overall heat transfer rate.

Figure 7-1 shows the schematic of the problem. It is modeled as a rectangle with a length-to-gap aspect ratio of 5 to minimize the edge effect near the midspan. The gap thickness between the upper and lower surfaces is 0.5 m. Sidewalls are excluded from the radiation process. The hot upper surface is maintained at a temperature of 400 K, and the cold lower surface has a constant wall temperature of 300 K. All the walls are treated as isothermal surfaces, and internal conduction heat transfer through these surfaces was not considered in the test.

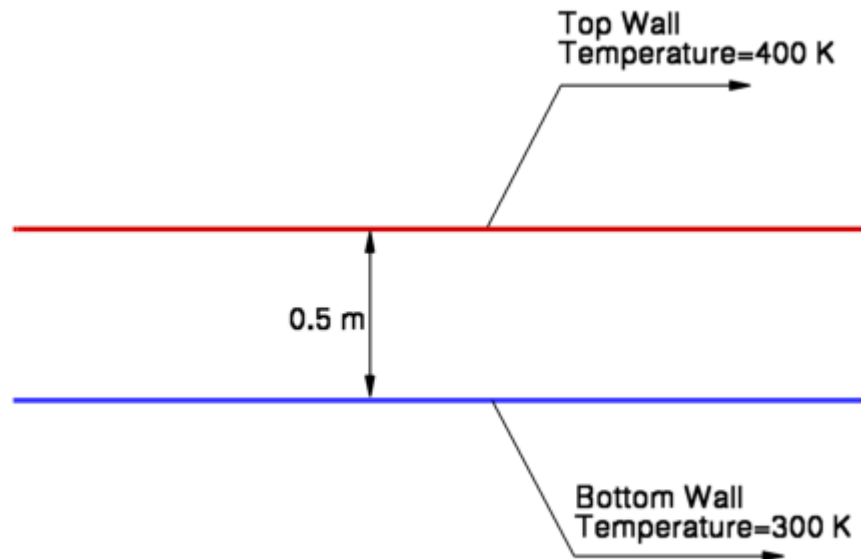


Figure 7-1. Schematic of Radiation Heat Transfer Between Parallel Surfaces

7.1.1 Theoretical Basis

The analytical solution for the present validation case is detailed in Incropera and DeWitt (1984).

Thermal flux between two parallel plates due to radiation is given by

$$q'' = \frac{\sigma(T_h^4 - T_c^4)}{\left(\frac{1}{\epsilon_h} + \frac{1}{\epsilon_c} - 1\right)} \quad (7-1)$$

where

T_h	—	Temperature of hot lower surface = 400 K
T_c	—	Temperature of cold upper surface = 300 K
ϵ_h	—	Surface emissivity of hot lower surface = 0.9
ϵ_c	—	Surface emissivity of cold upper surface = 0.9
σ	—	Stefan Boltzmann constant = $5.67 \times 10^{-8} \text{ W-m}^{-2}\text{-K}^{-4}$

In the absence of any convective flow, the fluid in the gap will act as a solid medium. The temperature distribution in the gap is given by

$$T(x) = T_c + x \left(\frac{T_h - T_c}{t} \right) \quad (7-2)$$

where

t	—	Gap thickness = 0.5 m
x	—	Distance along the gap (m)

In terms of dimensionless temperature and distance, Eq. (7-2) reduces to the form

$$T^* = x^* \quad (7-3)$$

where

T^*	—	Dimensionless temperature = $\left(\frac{T(x) - T_c}{T_h - T_c} \right)$
x^*	—	Dimensionless distance = $\left(\frac{x}{t} \right)$

7.1.2 Test Input

The test input for the present study uses the case file generated for Version 6.3. The solution domain shown in Figure 7-1 is meshed with a uniform grid without any clustering

because no steep gradient is expected due to the absence of any convective flow. The hot upper surface and the cold lower surface are included in the radiation heat transfer, and the sidewalls are excluded from the process. The gap between the plates is filled with air, but the flow equations are not solved and the media is treated as a stationary object. Most of the test is identical to that done for FLUENT Version 6.3, but here the discrete ordinate (DO) model is used instead of the S2S radiation model. In the DO model the radiative transport equation is solved for the absorbing, emitting and scattering medium for a number of solid angles. Input and results for the test case and research are on the attached media in the directory called /radflat-12.1/.

7.1.3 Expected Test Results

For acceptance, the computed flow field data should be able to predict the temperature distribution across the gap so that it lies within 10 percent of the overall range of the analytical solution. The net radiation heat exchanged between the surfaces should also be within 10 percent of the analytical value.

7.1.4 Test Results

Figure 7-2 shows the temperature variation across the gap near the center of the computational domain. The temperature decreases steadily and uniformly from the hot upper wall to cold lower wall. This pattern of temperature distribution indicates that there is no convective flow in the gap and the material inside the gap effectively behaved as a solid body. This is in agreement with the intended modeling approach for the present problem where the convective flow is disregarded, as the objective is to establish radiation as the only mode of heat transfer. The temperature pattern is also almost identical to that obtained using FLUENT.

The analytical and computed data for temperature distribution along the central line are shown in Figure 7-3 for a line across the center of gap. The figure also shows two dotted lines indicating the acceptable range of variation for the computed data. The computed and analytical solution almost overlap each other, and the computed results are well within the acceptable range.

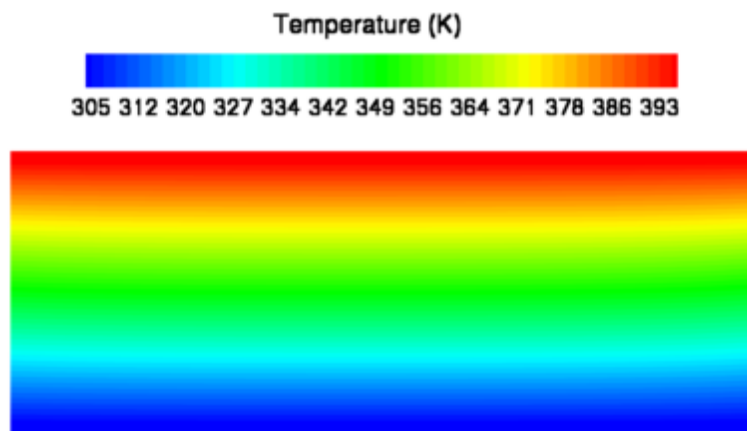


Figure 7-2. Temperature Contours Across the Gap Using DO Model in FLUENT Version 12.1

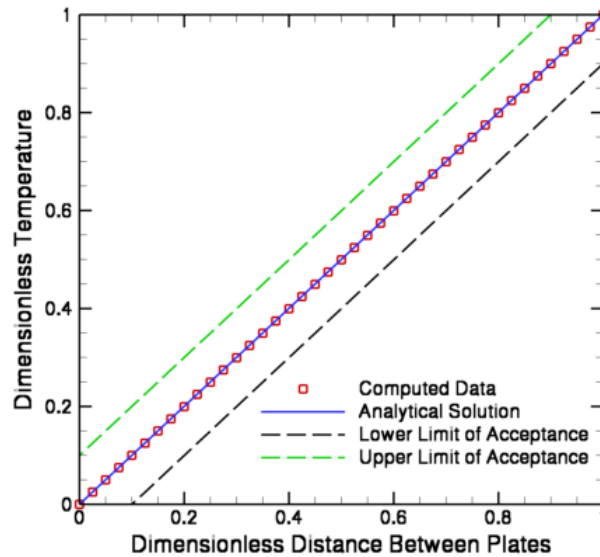


Figure 7-3. Comparison of Analytical and Computed Solution of Temperature Across the Gap Along with the Acceptance Limit of ± 10 Percent Using DO Model for FLUENT Version 12.1

The overall heat flux values the simulation predicts are compared to the analytical solution obtained from Eq. (7-2). The computed heat flux is 859.7 watts compared to the 811.84 watts obtained from the analytical solution. Therefore the deviation is around 6 percent, which is within the acceptable range of variation as per the validation requirement indicated in Section 7.1.3.

7.2 Radiation Between Two Concentric Cylinders

A one-dimensional analytical solution of radiation heat transfer between two concentric cylinders is used to validate the capability of FLUENT to model radiation heat transfer. The annulus between the concentric cylinders contains fluid at very low pressure, and the effect of gravity is neglected. This is done to maintain the radiation heat transfer process as the dominant mode of energy exchange between the outer and the inner walls and maintain a static medium in the annulus.

Figure 7-4 shows the schematic of the problem, which is similar to the validation test case described in Section 5-1. The geometric configuration of the domain shown in Figure 7-4 is identical to that of the validation case in Section 5-1, but the present test case does not have any fluid in the annulus between the concentric cylinders and the effect of gravity is neglected. This is done to maintain the radiation heat transfer process as the dominant mode of energy exchange between the outer and the inner walls and maintain a static medium in the annulus. The inner cylinder is at an elevated temperature of 700 K, and the outer cylinder is maintained at a constant temperature of 200 K. No internal heat generation was considered. Both the inner and outer cylinders participated in the radiation heat transfer process unlike the previous validation case, where the two sidewalls were not included in radiation heat transfer. Specifying a vacuum in the annulus ensured a transparent and nonparticipating medium in the annulus.

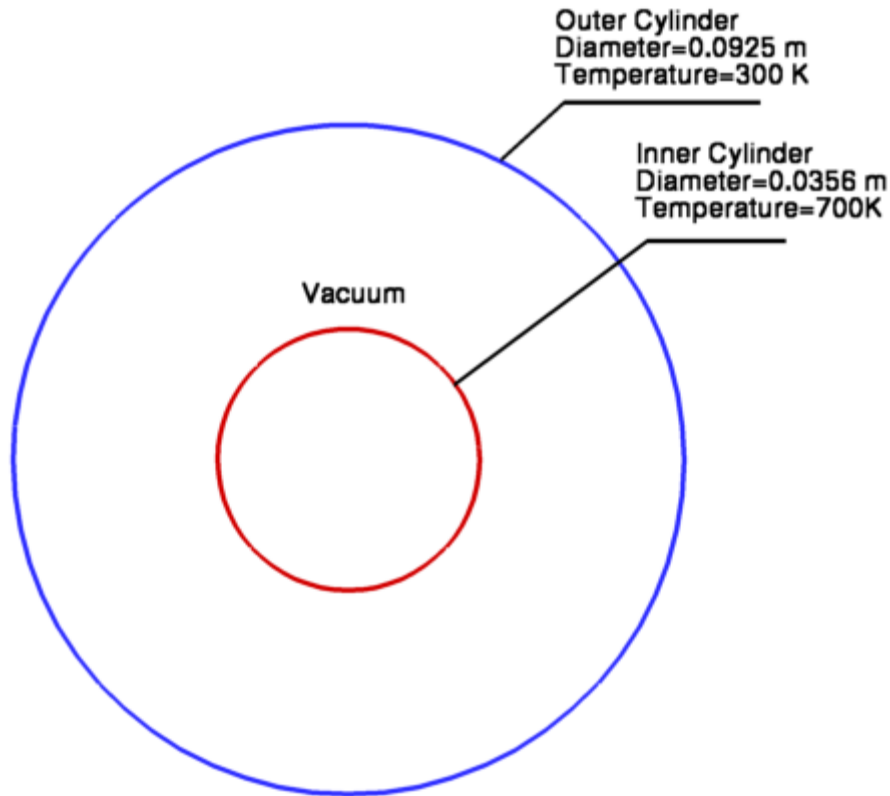


Figure 7-4. Schematic of Radiation Heat Transfer Between Concentric Cylinders

7.2.1 Theoretical Basis

The analytical solution for the present validation case is detailed in Incropera and DeWitt (1996).

Thermal flux between two concentric cylinders due to radiation is given by

$$q'' = \frac{\sigma(T_i^4 - T_o^4)}{\frac{1}{\varepsilon_i} + \frac{1 - \varepsilon_o}{\varepsilon_o} \left(\frac{r_i}{r_o}\right)} \quad (7-4)$$

where

T_o	—	Temperature of outer cylinder surface = 300 K
T_i	—	Temperature of cold upper surface = 700 K
ε_o	—	Surface emissivity of outer surface = 0.7
ε_i	—	Surface emissivity of cold upper surface = 0.9
σ	—	Stefan Boltzmann constant = $5.67 \times 10^{-8} \text{ W/m}^2\text{-K}^4$
r_o	—	Radius of outer surface (m)
r_i	—	Radius of inner surface (m)

$$T(r) = \frac{T_i - T_o}{\ln\left(\frac{r_i}{r_o}\right)} \ln\left(\frac{r}{r_o}\right) + T_o \quad (7-5)$$

In the absence of any convective flow, the fluid in the gap will act as a solid medium. The temperature distribution in the gap is given by

$$T^* = \frac{\ln\left[r^* \left(\frac{r_o - r_i}{r_o}\right) + \frac{r_i}{r_o}\right]}{\ln\left(\frac{r_i}{r_o}\right)} \quad (7-6)$$

where

r — Radial location in the annulus

In terms of dimensionless temperature and distance, Eq. (7-5) reduces to the form

where

T^* — Dimensionless temperature = $\left(\frac{T(r) - T_o}{T_i - T_o}\right)$

r^* — Dimensionless distance = $\left(\frac{r - r_i}{r_o - r_i}\right)$

7.2.2 Test Input

The case file generated to validate FLUENT Version 6.3 is used here. Note that the solution domain shown in Figure 7-5 is geometrically identical to the one described in Section 5-1, and as a consequence, the same mesh was used for the radiation study in this section. For the present validation study, the hot inner and cold outer surfaces are specified as isothermal walls at 700 K and 300 K, respectively. To simulate the effect of a vacuum in the annulus, it is simulated as air at extreme low pressure. To bypass the effect of convection and establish radiation as the dominant mode of heat transfer, flow equations are not solved. The surface-to-surface (S2S) radiation model of FLUENT is used. View factors for the geometry are calculated through the solver and are not supplied externally. Input and results for the test case are on the attached media in the directory called /k-g-rad-12.1/.

7.2.3 Expected Test Results

For acceptable performance, both the predicted temperature distribution across the gap and the net radiation heat exchanged between the surfaces should be within 10 percent of the overall range of the analytical solution.

7.2.4 Test Results

Figure 7-5 shows the temperature distribution in the gasp. The temperature values decrease constantly in the radial direction. This is expected as there is no other form of heat transfer except radiation and the fluid in the annular space does not participate in either conduction or radiation. This is similar to the observation made in the previous study and is consistent with the analytical finding described in Section 7.2.1.

Figure 7-6 shows the variation of computed temperature across the annulus and compares it with an analytical solution. The figure also shows two dotted lines indicating the acceptable range of variation of the computed data, which are obtained by adding the deviation to the analytical solution. The results are similar to those obtained in the previous study for validating FLUENT Version 6.3. The computed and analytical solutions are in excellent agreement with each other, and the computed results lie within the acceptable range of deviation from the analytical data, indicating that FLUENT Version 12.1 effectively simulated radiation using the S2S method.

The analytical solution of overall heat flux values is obtained from Eq. (7-4) and is compared with the computed value. The computed and analytical heat fluxes are 1065.26 and 1029.83 watts, respectively. This shows that the simulated value deviates only by 3.33 percent from analytical data, which is within the acceptable range of variation as per the validation test plan as discussed in Section 7.2.3.

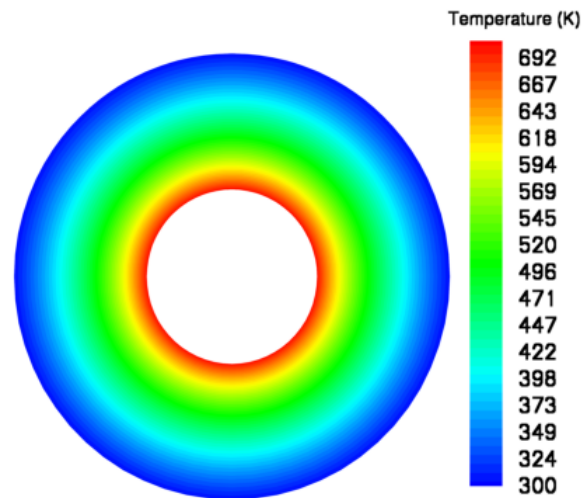


Figure 7-5. Temperature Contours Annulus Using S2S Model in FLUENT Version 12.1

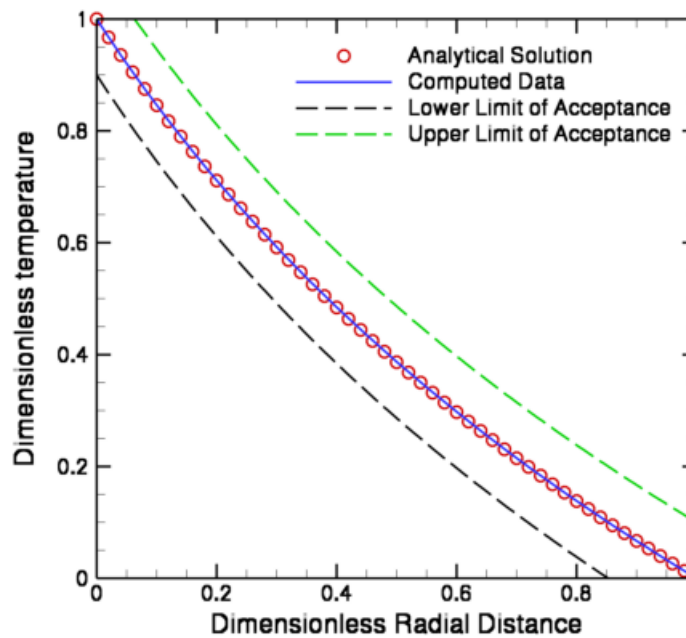


Figure 7-6. Comparison of Analytical and Computed Solution of Temperature Across the Annulus Using FLUENT Version 12.1. (Acceptance Limit is Within ± 10 Percent of Analytical Value)

8 SPECIES TRANSPORT AND MULTIPHASE FLOWS

Two test cases to validate the capability of the FLUENT solver in simulating multiphase flows are presented in this chapter. Standard FLUENT has a number of techniques to model multiphase flows using the discrete particle method, Eulerian model, mixture model, and the volume of flow approach. Based on the potential application of the solver, the validation test cases discussed in this chapter focus on non-reacting species transport technique and solve two phase flows.

8.1 Diffusion Through Mixture Column at Constant Pressure and Temperature

Analytical solution of diffusion in the binary gas mixture provides a method to validate the accuracy of FLUENT for multispecies flows. The test case assumes constant pressure and temperature throughout the solution domain.

The computational domain and boundary conditions are shown Figure 8-1. A mixture of water vapor and air fills the domain. The mass fractions of water vapor at the left and right wall are fixed at 0.9 and 0.1, respectively. This difference in water vapor mass fraction produces a concentration gradient, and water vapor travels from the left wall toward the right wall due to diffusion. For a steady one-dimensional condition with no chemical reactions, the mass flux or molar flux of water vapor must be constant. As the pressure and temperature at every point of the flow are constant, the molar concentration is also constant and the sum of the mass fraction of air and water vapor at any point should be equal to unity. To maintain this condition, air should also diffuse from the right to the left of the domain. However, a steady-state condition can only be maintained if the leftward diffusion of air is counterbalanced by a rightward bulk motion. This is to ensure that the absolute flux of air is zero at any location. Hence there will be diffusive mass transfer for both air and water vapor, but a bulk flow from right to left to ensure a zero flux of air at any cross section of the domain.

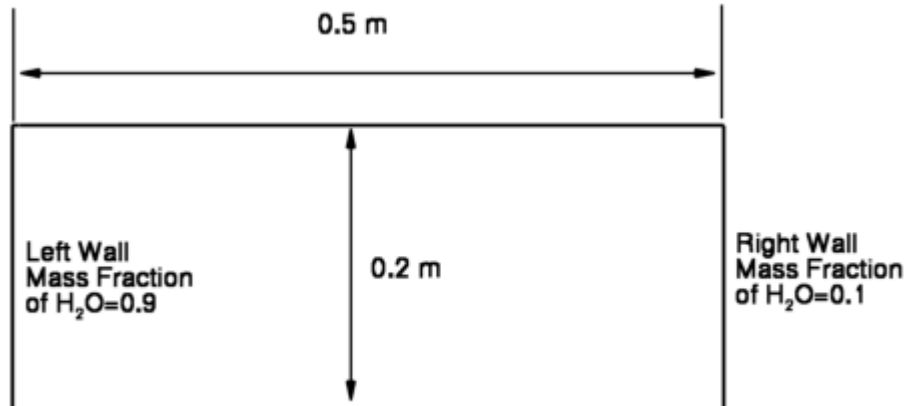


Figure 8-1. Schematic of Diffusion in Mixture Column

8.1.1 Theoretical Basis

The analytical solution for the present validation case is detailed in Incropera and Dewitt (1996) and in Bird, et al. (1960). The transport equation for water vapor in a one-dimensional domain with bulk mixture flow can be written as

$$N'''_{H_2O} = -\rho D \frac{dx_{H_2O}}{dx} + x_{H_2O} N'''_{H_2O} \quad (8-1)$$

where

N'''_{H_2O}	—	Mass flux of H ₂ O vapor from left to right of the domain (kg/m ² –s)
ρ	—	Total density (kg/m ³)
x_{H_2O}	—	Mass fraction of H ₂ O vapor
D	—	Diffusion coefficient (m ² /s)
x	—	Distance from left wall (m)

Eq. (8-1) can be rearranged in the form

$$N'''_{H_2O} = -\frac{\rho D}{1 - x_{H_2O}} \frac{dx_{H_2O}}{dx} \quad (8-2)$$

Under steady-state conditions

$$\frac{dN'''_{H_2O}}{dx} = 0 \quad (8-3)$$

So, for steady-state conditions, Eq. (8-2) could be written as

$$\frac{d}{dx} \left(\frac{1}{1 - x_{H_2O}} \frac{dx_{H_2O}}{dx} \right) = 0 \quad (8-4)$$

The boundary conditions for the validation test case could be given as

$$x = 0; \quad x_{H_2O} = 0.9;$$

$$x = 0.5; \quad x_{H_2O} = 0.1.$$

The solution of Eq. (8-4) is given by

$$x_{H_2O} = 1 - 0.1(9)^{x/0.5} \quad (8-5)$$

As the sum of the mass fractions of air and water vapor is unity, the mass fraction variation of air could be given as

$$x_{air} = 0.1(9)^{x/0.5} \quad (8-6)$$

8.1.2 Test Input

The mesh and case file used for the validation exercise of Version 6.3 is used here. The mesh file was loaded inside the workbench to impose boundary conditions using ANSYS Meshing. The domain and boundary conditions related to the test case were already discussed in Section 8.1. Uniform grid spacing without any clustering of grids is used to mesh the domain. The problem is modeled in a 2D domain, and the incompressible Navier-Stokes equations are solved without any turbulence models, because the flow is expected to be laminar. Species transport equations with inlet diffusion and a diffusion energy source are solved for the vapor phase. The working fluid is specified as a mixture of water vapor and air, and the fluid density was determined using the volume-weighted mixing law. The input and results file for this test case are on the attached media in the drive /BSL/single-phase. A number of simulations are also done using the multiphase flow subroutine, but this is not discussed in this report. Relevant files are in the directory /BSL/multiphase.

The test case setup used to validate Version 12.1 is slightly different from that used to validate Version 6.3. Previously, a user-defined diffusion coefficient was used to model the one-dimensional mass transfer inside the domain. In the present scenario, the wall boundary condition was modified to account for mass addition or removal from the system due to specification of constant flux boundary condition at the wall.

The existing case uses air and water vapor mixture in a constant pressure and volume chamber to study the diffusion process. It is possible to repeat this exercise with any combination of fluids. The species mass flux at the interface is given as

$$\dot{m}''_{air} = \rho x_{air} v - \rho D \frac{\partial x_{air}}{\partial n} \quad (8-7)$$

$$\dot{m}''_{h_2o} = \rho x_{h_2o} v - \rho D \frac{\partial x_{h_2o}}{\partial n} \quad (8-8)$$

where

x_{H_2O}	—	Mass fraction of H ₂ O vapor
x_{air}	—	Mass fraction of air
n	—	Vector in normal direction
\dot{m}''_{air}	—	Mass flux of air
\dot{m}''_{h_2o}	—	Mass flux of water vapor

Equations (8-7) and (8-8) are modified to account for source terms in the near-wall region due to the addition of water vapor species at a constant rate. These source terms

are coded in a user defined subroutine, compiled using the GNU c-compiler, and then hooked into the FLUENT Version 12.1 solver.

8.1.3 Expected Test Results

The predicted water vapor mass fraction across the domain will be compared with the analytical solution. The computed variation of mass fraction values of different phases should be within 10 percent of the analytical value.

8.1.4 Test Results

Figure 8-2 (a,b) shows the variation of the water vapor mass fraction in the domain using FLUENT Versions 12.1 and 6.3 of FLUENT, respectively. In general, it can be observed that there is a one-dimensional variation of mass fraction with a higher value near the left wall and a lower value at the right wall. Additionally, this variation is not linear in nature, confirming that the computed solution is able to qualitatively capture the species distribution. There is, however, some clear distinction in the species distribution pattern between the solutions. Figure 8-2(a) clearly shows a distorted bulge of the contour lines near the center of the domain, whereas for the Version 6.3 solution, the contour patterns almost follow a regular vertical pattern. This is because the Version 6.3 solution was obtained using the modified diffusion coefficient and any edge or wall effect was eliminated. The theoretical distribution described in Section 9.1.1 does not consider wall effect. The modified diffusion coefficient provided a solution that was closer to the theoretical distribution, but in reality, the diffusion coefficient does not vary across the flow domain. Instead the mass transfer and adjustment process near the wall causes species movement and the wall effect on flow pattern cannot be neglected for a realistic flow situation. The species distribution near the centerline for Version 12.1 was least

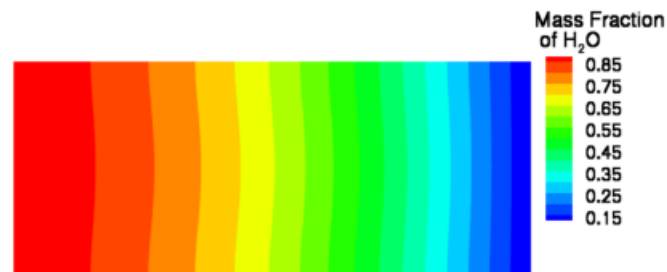
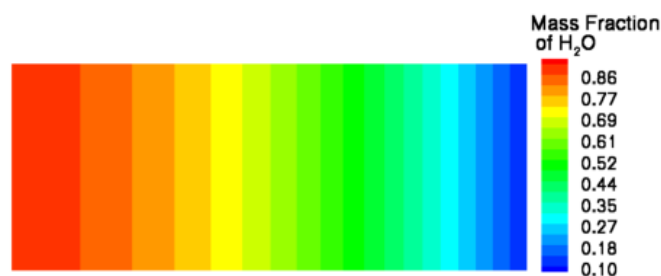


**Figure 8-2. Water Vapor Mass Fraction Variation in the Flow Field Using
(a) Version 12.1 and**



(b) Version 6.3

influenced by the wall and provides the closest approximation to the theoretical distribution as will be shown in next two figures.

Figure 8-3 (a,b) compares the computed and analytical solutions of the water vapor distribution across the domain from the left wall to the right wall along the centerline for Versions 12.1 and 6.3, respectively. The distance from the left wall is nondimensionalized with respect to the gap length between the right and left walls. The computed values of the mass fraction are in reasonable agreement with the analytical solution. Both the analytical and computed data show similar trends, but the agreement is closer near the walls. At the middle of the computational domain, the simulated results deviate from the computational results, but the maximum deviation is still within acceptable limits. Both Versions 12.1 and 6.3 provide almost identical results, and the edge effects are minimal along the centerline.

Figure 8-4 (a,b) compares the computed and analytical solutions of the air mass fraction distribution across the domain from the left wall to the right wall along the centerline for Versions 12.1 and 6.3, respectively. The results obtained using these two solvers are almost identical and are within the acceptable limits specified in Section 8.1.3.

Based on the comparison between the theoretical distribution and computational values, it can be concluded that the solution lies within acceptable limits and the solver is suitable for simulating species transport problems.

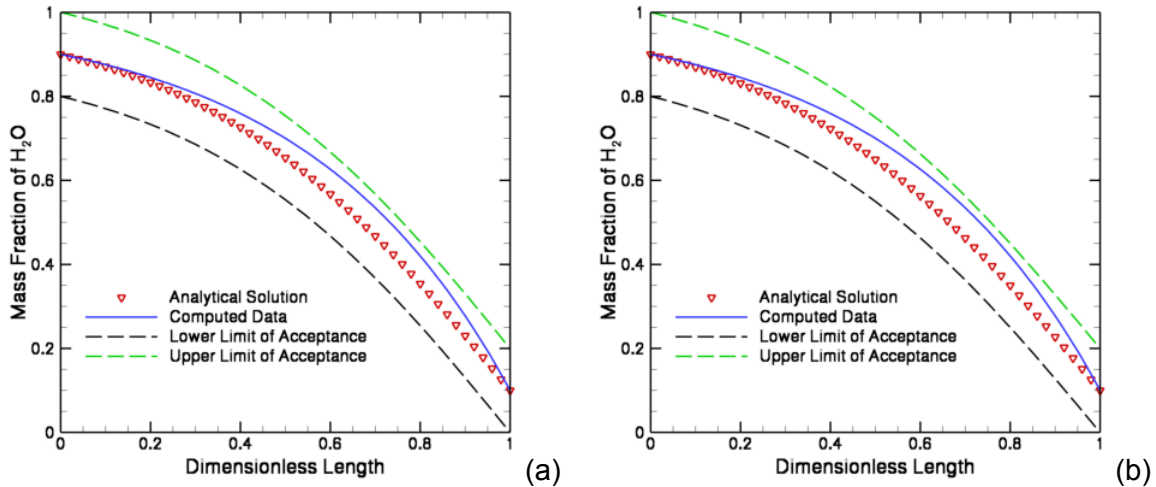


Figure 8-3 (a,b). Comparison of Analytical and Computed Solution of Mass Fraction of Water Vapor. (a) Version 12.1 and (b) Version 6.3

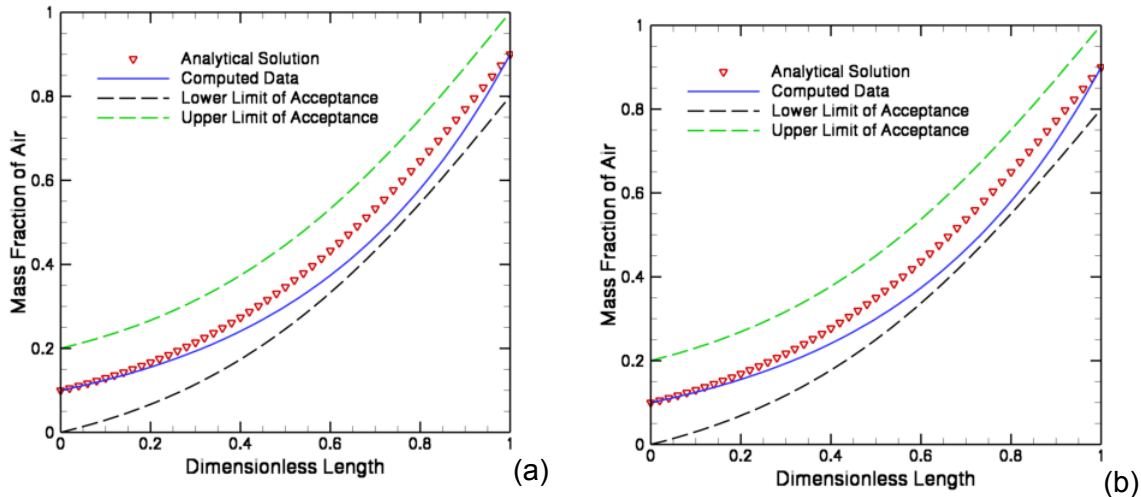


Figure 8-4 (a,b). Comparison of Analytical and Computed Solution of Mass Fraction of Air. (a) Version 12.1 and (b) Version 6.3

8.2 Condensation of Water Vapor Over Flat Plate

Sparrow, et al. (1967) provided an analytical solution for condensation of water vapor from humid air over a flat plate. This analytical solution was used as a validation benchmark to assess FLUENT's capability to model moisture transport and condensation including multiphase flow and interphase mass transfer. The proposed validation test is also archived and documented as an application brief by Fluent, Inc.³ The application brief only includes single-phase species transport with film condensation at the wall. It does not consider the effect of volumetric condensation when the local water vapor mass fraction exceeds the saturation limit in certain locations. The condensation module ANSYS-FLUENT provides has been modified to include the effect of volumetric condensation to establish local equilibrium and has been validated using this test case. Hence, a modified user-defined function was used to validate FLUENT Version 12.1.

When a mixture of air and water vapor contacts a surface at a temperature below the saturation value, condensation takes place on the cold surface, forming a liquid film that moves due to shear and gravity forces. Air accumulates at the condensed liquid and air-vapor mixture interface during the condensation process, slowing down the rate of condensation. A number of factors, including the complex heat transfer process through the air and liquid film, determine the rate of condensation. For the present test case, the mass fraction of air in the free stream is high and the thermal resistance of the liquid film formed due to condensation is small. Under this circumstance, the diffusion of water vapor through the accumulated air in the interface between liquid and vapor primarily governs the condensation rate. This test will model the condensation process and compare the computed distribution liquid water mass with an analytical solution at the cold wall. It will also model the volumetric condensation process to establish localized equilibrium in the domain that ensures that water vapor mass fraction does not exceed saturation value.

³Private communication with ANSYS Inc. technical representative.

The computational domain, grid, and boundary conditions for the condensation problem are shown Figure 8-5. A mixture of water vapor and air is specified as the working fluid in the domain. The free stream velocity is specified at the velocity inlet of the domain along with temperature and mass fraction of water vapor. A pressure outlet boundary condition with specified backflow temperature and water vapor mass fraction is specified at the downstream outlet as well as at the top of the domain. A number of customized source terms for the continuity, momentum, energy, and species equations are introduced through user-defined functions to model the effect of mass removal due to condensation at the cold bottom wall. To capture the boundary layer and the condensation process, grids are clustered near the bottom wall.

8.2.1 Theoretical Basis

Sparrow, et al. (1967) presents the analytical solution for condensation of humid air in a flat plate. The present validation test case simulates the same problem and models the condensation process along the cold wall. ANSYS Inc.⁴ developed user-defined functions to model the condensation process and incorporate the effect on the flow and transport equations. Assumptions for the condensation modeling include the following:

1. Thermodynamic equilibrium occurs at the liquid–mixture interface.
2. The condensed water at the wall does not contain any dissolved air.
3. Film condensation takes place on the cold surface; dropwise condensation is neglected.
4. The liquid film formed on the surface offers viscous resistance to the mixture but offers no thermal resistance.

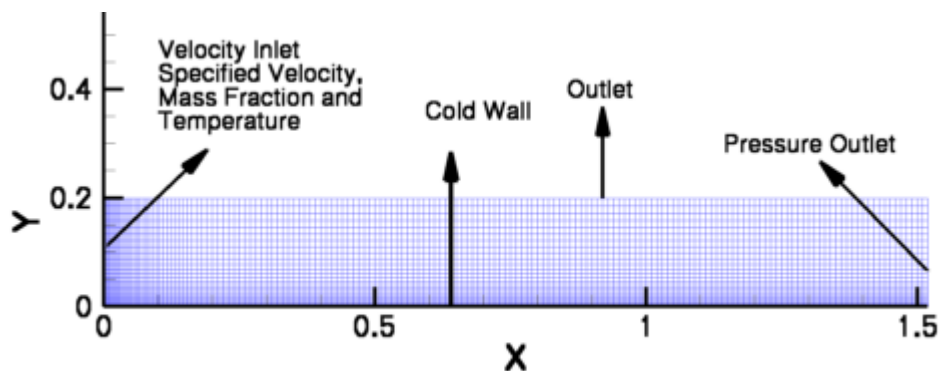


Figure 8-5. Schematic for Condensation of Humid Air Over Flat Plate

⁴ Private communication with ANSYS Inc. technical representative.

A number of assumptions are also made to model the volumetric phase change process that include the following:

1. The condensed water in a particular cell or in the domain does not form large bubbles that will rain out. Instead it will be floating with the existing mixture and diffusing through it as mist.
2. Slip velocity between the water droplets formed, and the mixture phase is neglected.
3. Volumetric evaporation is not considered in the simulations, because for the cases considered, it will be negligible. Moreover, the relative humidity is likely to be very high in most of the domain resulting in minimal volumetric evaporation.
4. The modules are developed for the mixture multiphase model of FLUENT and will not work with volume of fluid or Eulerian models.

The species mass flux equation for water vapor (Bird, et al.,1960) at the cold wall could be written as

$$m'''_{H_2O} = -\rho D \frac{dx_{H_2O}}{dy} + x_{H_2O} \rho v \quad (8-7)$$

where

m'''_{H_2O}	—	Volumetric mass source removed from the domain that condenses on the wall (kg/m ²)
ρ	—	Mixture density (kg/m ³)
x_{H_2O}	—	Mass fraction of H ₂ O vapor
D	—	Diffusion coefficient (m ² /s)
y	—	Vertical distance from bottom wall (m)
v	—	Normal fluid velocity at the condensed water mixture interface (m/s)

Eq. (8-7) can be modified in the form

$$m'''_{H_2O} = -\frac{x_{H_2O}}{x_{H_2O} - 1} \rho D \frac{dx_{H_2O}}{dy} \frac{A_{cellwall}}{V_{cell}} \quad (8-8)$$

where

$A_{cellwall}$	—	Cell face area at the wall (m ²)
V_{cell}	—	Volume of the cell (m ³)

Eq. (8-8) is used to formulate the source terms used in the mass, momentum, energy, and species transport equations.

The interphase mass transfer process, where the water vapor forms liquid water droplet mist, is modeled using Eq. (8-9), which describes the mass transfer rate required to achieve local thermodynamic equilibrium.

$$\dot{m} = f_{relax} \times \rho_{mixture}(m_{f,cell} - m_{f,saturated}) \quad (8-9)$$

where

f_{relax} — Relaxation factor
 $\rho_{mixture}$ — Mixture density
 $m_{f,cell}$ — Cell water vapor mass fraction
 $m_{f,saturated}$ — Cell saturated mass fraction at cell temperature

f_{relax} acts simultaneously as a rate constant as well as a numerical underrelaxation parameter. The numerical experiments also showed that the relaxation factor is highly dependent on the flow and turbulence. For natural convection flow problems, it can be as high as 0.8–0.95, whereas for forced convection problems, it is almost restricted to 0.1–0.4 depending on other flow parameters.

8.2.2 Test Input

The computational domain, grids, and boundary conditions relevant to the test case were discussed in Section 8.2. The test case is modeled as a 2D steady laminar two-phase flow problem, and the incompressible Navier-Stokes equations are solved without any turbulence models. Species transport equations with inlet diffusion and a diffusion energy source are solved for the vapor phase. Two different velocities with fixed water vapor concentration at the inlet are studied, and results are compared with experimental data. The working fluid is specified as a mixture of water vapor and air, and fluid density is determined using the volume-weighted mixing law. The customized, user-defined function to incorporate the source terms is compiled and hooked to the mass, momentum, energy, and species transport equations using the standard FLUENT interface. The user-defined functions, mesh, and the basic case file were obtained from ANSYS Inc.⁵ and later modified to include the modifications needed for multiphase flows. Input and results for this test case are on the attached media in the directories /conden-12.1/single-phase and /conden-12.1/multiphase for single and multiphase flows, respectively.

8.2.3 Expected Test Results

The overall flow field species fraction distribution should be in agreement with the general understanding of channel flow and should qualitatively predict the mass fraction distribution pattern in the flow field and near the wall. The computed condensation mass fraction at the wall should not deviate more than 25 percent from the overall range calculated from the analytical solution for both single- and multiphase-flow solutions. In addition, the multiphase model should demonstrate that it was able to achieve localized equilibrium that can be demonstrated through a relative humidity or saturation condition. For acceptance, the maximum level of supersaturation should not exceed 10 percent of the saturation value.

⁵ Private communication with ANSYS Inc. technical representative.

8.2.4 Test Results

Figures 8-6 through 8-9 show results obtained using the single-phase species transport model with film condensation at the wall, whereas Figures 8-10 through 8-13 highlight results obtained from multiphase flow simulations that account for interphase mass transfer due to volumetric condensation. Both these test cases were run for two different mixture inlet velocities of 1 m/s and 0.1 m/s, but the mass fraction of vapor in the mixture was fixed at 0.47967.

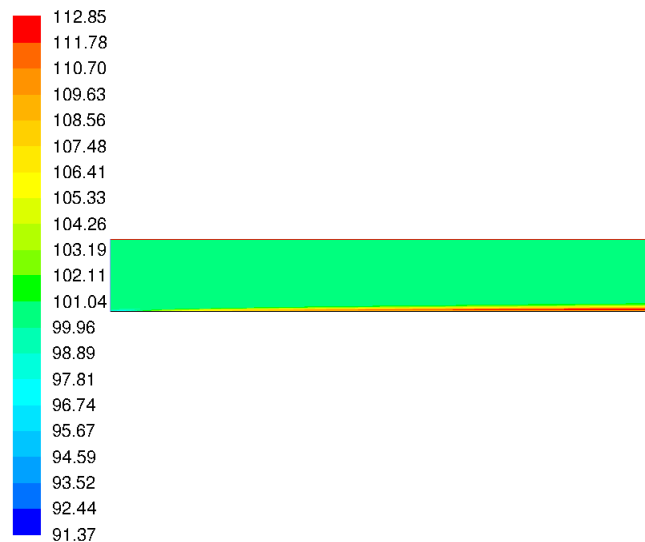
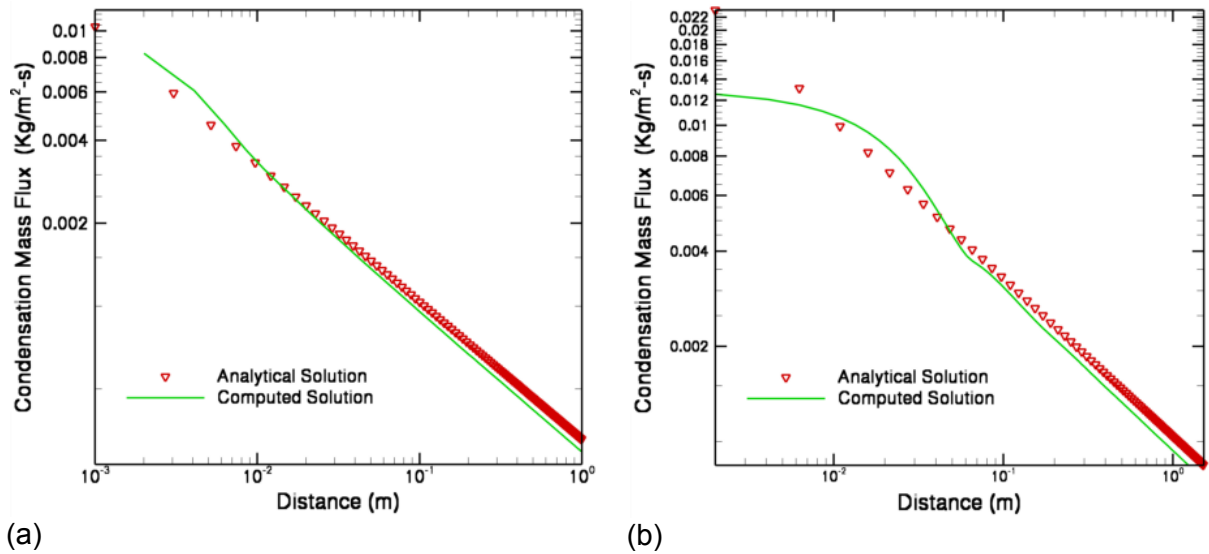
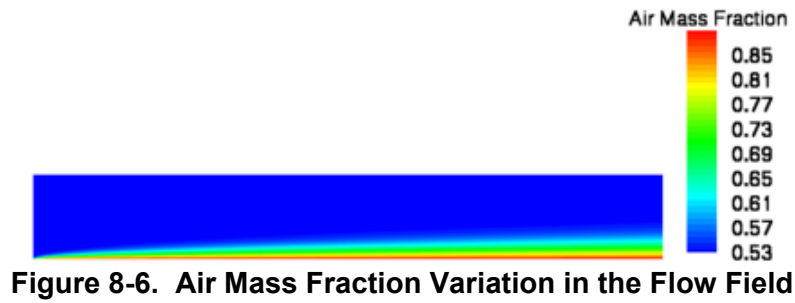
8.2.4.1 Test Results for Single-Phase Species Transport

The air mass fraction contours for an inlet velocity of 1 m/s are shown in Figure 8-6. The thickness of air mass fraction increases along the cold wall because the mixture loses water vapor due to condensation and the mass fraction of water vapor in the mixture decreases. Consequently, the mass fraction of air in the mixture increases near the bottom wall of the domain. This is consistent with the understanding of the physics of film condensation on cold flat plates.

Figure 8-7 (a,b) compares condensed mass flux at the cold bottom wall for an inlet velocity of 0.1 m/s. In the downstream region, the pattern of the computed results is in good agreement with the analytical solution, though the computed result slightly underpredicts the data. The analytical and computed solutions have some deviation near the leading edge of the plate, though near the trailing edge, the deviations do not exceed 10 percent of the overall range. The computed solutions do not take into account the boundary layer development and assume a fully developed layer from the leading edge. The leading edge results should be excluded from comparison, and the study is considered validated for the downstream flow. The deviation in the trailing edge occurs because the analytical solution makes certain assumptions regarding the boundary layer thickness near the plate leading edge that are different from the simulated case. This deviation is within an acceptable range as described in the software validation test plan.

Figure 8-8 compares the computed and analytical solution for an inlet velocity of 1 m/s. It shows the same trend as the previous test case with a different inlet velocity. Results show some deviation between simulated and analytical solution that is within 10 percent based on the total range and is within the acceptable range, as described in Section 8.2.3.

Figure 8-8 shows the contours of relative humidity for the entire flow domain for an inlet velocity of 1 m/s. Although the majority of the domain is either at a saturated or unsaturated condition, a thin area near the condensation zone shows supersaturation. As mentioned in Section 8.2.1, the single-phase simulations do not consider volumetric condensation, where the excess water vapor that causes supersaturation is allowed to condense and form liquid droplet water. In reality, some of the water that exceeds the local saturation limit will condense and form mist droplets that will diffuse through the flow. This highlights the deficiency of using a single phase with a species transport model in capturing the actual physical process.



8.2.4.2 Test Results for Multiphase Transport with Volumetric Condensation

Figure 8-9 shows the air mass fraction distribution in the domain. It is similar to that shown in Figure 8-6 for single-phase flow. This can be attributed to the fact that the volumetric water condensation rate is significantly smaller compared to the wall condensation rate to affect the species distribution pattern. Due to the high wall condensation rate, the air mass fraction near the bottom cold wall gets affected. Inside the domain, away from the wall, volumetric condensation is the only mechanism that can affect species distribution. As the volumetric condensation rate is orders of magnitude less compared to wall condensation, the species distribution appears to be unaffected.

Figure 8-10 (a,b) shows the wall condensation mass flux for two different test runs for multiphase flow modeling. For both runs, computed results reasonably predict the experimental data. However, unlike the test cases described in Section 8.4.2.1 in connection with single-phase flows, where the computed results slightly underpredicted the condensation rate, here the computed solution slightly overpredicts it. The disparity between computed and analytical solution in upstream region is more compared to the single phase solution. This can be attributed to a number of factors.

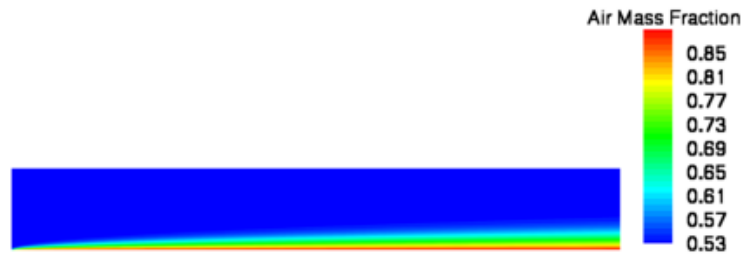


Figure 8-9. Air Mass Fraction Variation in the Flow Field with Multiphase Flow and Inlet Velocity = 1 m/s

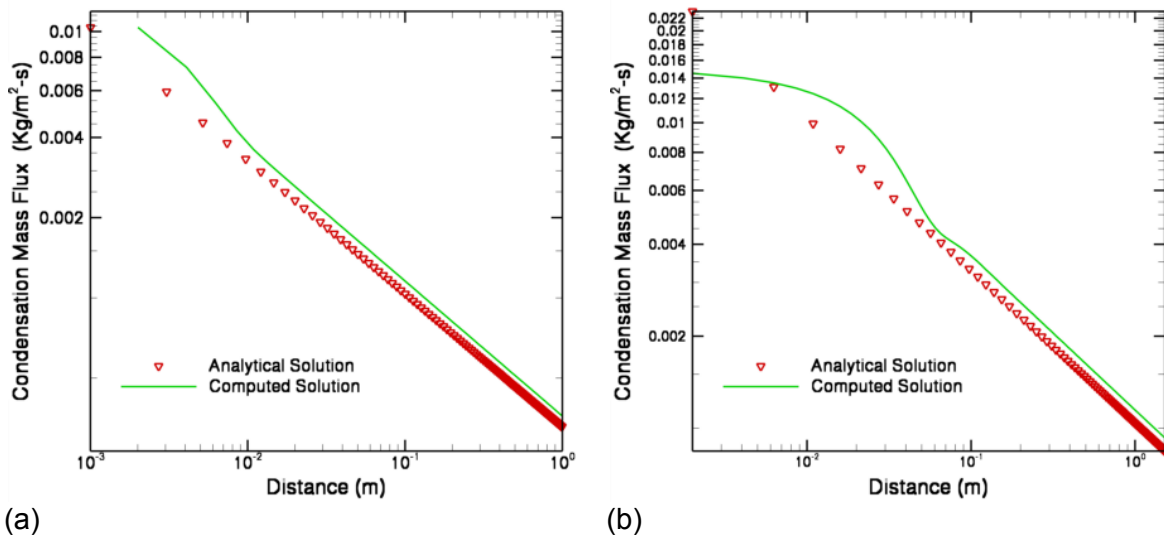


Figure 8-10 (a,b). Comparison of Analytical and Computed Results for Condensation Mass Flux for Inlet Velocity Using Multiphase Flow Modeling. (a) Equals 0.1 m/s and (b) Equals 1 m/s

1. The analytical solution was derived for wall condensation only and did not consider volumetric condensation. Therefore, some disagreement between the multiphase flow solutions that consider volumetric condensation with experimental data was expected.
2. Removal of water vapor from the mixture phase may have caused a steeper gradient of species concentration, causing higher diffusion flux of water vapor toward the wall.
3. The volumetric condensation process affects the species distribution of water vapor near the cold wall and can affect the diffusion flux of water vapor through the boundary layer that ultimately affects the condensation rate.
4. As explained in Section 8.4.2.1, a number of assumptions were made in the analytical solution near the flat plate leading edge regarding boundary layer development that was not present in the computational solution. The boundary layer development in the computational solution did not follow the prescribed profile specified for the analytical solution.

Figure 8-11 shows the relative humidity contours for the flow domain, where most of the domain is in saturation condition and only a thin band of area near the cold wall exhibits some degree of supersaturation. The supersaturation values are, however, less than 10 percent of the saturation condition and are within the acceptable limit as prescribed in Section 8.2.3.

Based on the results obtained from the previously mentioned tests, it can be concluded that the single-phase simulations using FLUENT Version 12.1, along with the user-defined routine, can be used to simulate the wall condensation rate. The multiphase modification of the user-defined routines can be used to calculate both wall condensation and volumetric condensation rate throughout the domain. It can also be used to calculate the species fraction distribution and relative humidity in the flow domain.

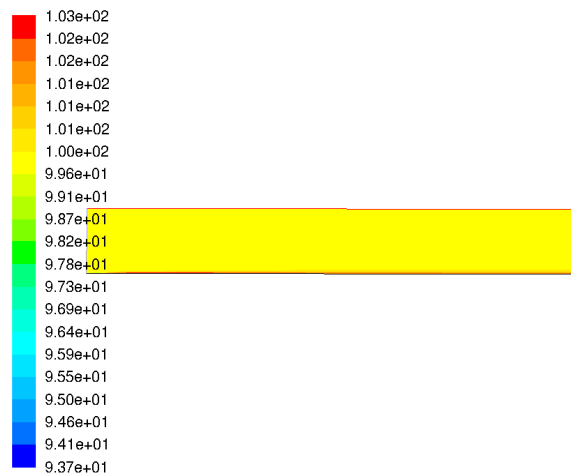


Figure 8-11. Relative Humidity Contours for Simulation with Multiphase Species Transport and Inlet Velocity = 1 m/s

9 INDUSTRY EXPERIENCE

None.

10 NOTES

None.

11 REFERENCES

- ANSYS Inc. "FLUENT User's Guide." Version 12.1. Canonsburg, Pennsylvania: Fluent, Inc. 2009a.
- . "ANSYS-Workbench User's Guide." Version 12.1. Canonsburg, Pennsylvania: Fluent, Inc. 2009b.
- . "ANSYS-Design Modelers User's Guide." Version 12.1. Canonsburg, Pennsylvania: Fluent, Inc. 2009c.
- . "ANSYS-Meshing User's Guide." Version 12.1. Canonsburg, Pennsylvania: Fluent, Inc. 2009d.
- . "ANSYS-CFD-Post User's Guide." Version 12.1. Canonsburg, Pennsylvania: Fluent, Inc. 2009e.
- Anderson, J.D. *Modern Compressible Flow*. New York City, New York: McGraw Hill Inc. 1984.
- Baughn, J.W., M.A. Hoffman, R.K. Takahashi, and B.E. Launder. "Local Heat Transfer Downstream of an Abrupt Expansion in a Circular Channel with Constant Wall Heat Flux." *Journal of Heat Transfer*. Vol. 106. pp. 789–795. 1984.
- Bechtel SAIC Company, LLC. "In-Drift Natural Convection and Condensation." MDL-EBS-MD-000001. Rev. 00. Las Vegas, Nevada: Bechtel SAIC Company, LLC. 2004.
- Bird, R.B., W.E. Stewart, and E.N. Lightfoot. *Transport Phenomena*. New York City, New York: John Wiley & Sons. 1960.
- Bush, R.H., G.D. Power, and C.N. Towne. "WIND: The Production Flow Solver of the NPARC Alliance." 36th Aerospace Sciences Meeting and Exhibit. Reno, Nevada, January 12–15, 1998. AIAA-98-0935. Published on CD-ROM. Reston, Virginia: AIAA. 1998.
- Das, K. and D. Basu. "Software Validation Test Plan for FLUENT Version 6.3." San Antonio, Texas: CNWRA. 2007.
- Das, K. and D. Basu. "Software Validation Report for FLUENT Version 6.3." San Antonio, Texas: CNWRA. 2008.
- Driver, D.M. and H.I. Seegmiller. "Features of Reattaching Turbulent Shear Layer in Divergent Channel Flow." *AIAA Journal*. Vol. 23. pp. 162–171. 1985.
- Fluent Inc. "FLUENT Validation Manual." Version 6.3. Lebanon, New Hampshire: Fluent Inc. 2007a.

———. “FLUENT 6.3 Validation Solution Files.” Lebanon, New Hampshire: Fluent Inc. 2007b.

Georgiadis, N., D. Yoder, and W. Engblom. “Evaluation of Modified Two Equation Turbulence Models for Jet Flow Predictions.” 44th AIAA Aerospace Sciences Meeting and Exhibit. Reno, Nevada, January 9–12, 2006. AIAA-2006-490. Published on CD ROM. Reston, Virginia: AIAA. 2006.

Goebel, S.G. and J.C. Dutton. “Experimental Study of Compressible Turbulent Mixing Layers.” *AIAA Journal*. Vol. 29, No. 4. pp. 538–546. 1991.

Green, S. and C. Manepally. “Software Validation Test Plan for FLOW-3D Version 9.” Rev. 1. San Antonio, Texas: CNWRA. 2006.

Holman, J.P. *Heat Transfer*. 9th Edition. New York City, New York: McGraw-Hill. 2002.

Incropera, F.P. and D.P. Dewitt. *Fundamentals of Heat and Mass Transfer*. 4th Edition. New York City, New York: John Wiley & Sons, Inc. 1996.

Kuehn, T.H. and R.J. Goldstein. “An Experimental Study of Natural Convection Heat Transfer in Concentric and Eccentric Horizontal Cylindrical Annuli.” *ASME Journal of Heat Transfer*. Vol. 100. pp. 635–640. 1978.

Kuehn, T.H. and R.J. Goldstein. “An Experimental Study and Theoretical Study of Natural Convection in the Annulus Between Horizontal Concentric Cylinders.” *Journal of Fluid Mechanics*. Vol. 74, Part 4. pp. 695–719. 1976.

LeFevre, E.J. “Laminar Free Convection from a Vertical Plane Surface.” Proceedings of 9th International Congress of Applied Mechanics, Brussels. Vol. 4. p. 168. 1956.

Ostrach, S. “An Analysis of Laminar-Free Convection Flow and Heat Transfer About a Flat Plate Parallel to the Direction of the Generating Body Force.” NASA TR-1111. Cleveland, Ohio: NASA. 1953.

Ozisik, M.N. *Basic Heat Transfer*. New York City, New York: McGraw-Hill. 1977.

Schlichting, H. *Boundary Layer Theory*. New York City, New York: McGraw Hill Inc. 1960.

Sparrow, E.M., W.J. Minkowycz, and M. Saddy. “Forced Convection Condensation in the Presence of Noncondensables and Interfacial Resistance.” *International Journal of Heat and Mass Transfer*. Vol. 10. pp. 1,829–1,845. 1967.

Todreas, N. and M.S. Kazimi. *Thermal Hydraulic Fundamental and Elements of Thermal Hydraulic Design*. Vols. I–II. New York City, New York: Hemisphere Publishing Corporation. 1990.